MOLECULAR DYNAMICS SIMULATION STUDIES OF FRACTURE IN TWO DIMENSIONS

by

BENITO de CELIS

SUBMITTED IN PARTIAL FULFILLMENT
OF THE REQUIREMENTS FOR THE
DEGREES OF

NUCLEAR ENGINEER

and

MASTER OF SCIENCE

at the

MASSACHUSETTS INSTITUTE OF TECHNOLOGY

May 1980

© Massachusetts Institute of Technology 1979

Signature of Author _____
Department of Nuclear Engineering
May 29, 1980

Certified by _____
Sidney Yip, Thesis Supervisor

Certified by _____
Ali Argon, Thesis co-Supervisor

Accepted by _____
Allan F. Henry, Chairman, Departmental Graduate Committee

ARCHIVES
MASSACHUSETTS INSTITUTE
OF TECHNOLOGY

JUN 13 1980

LIBRARIES

Report Documentation Page

Form Approved
OMB No. 0704-0188

Public reporting burden for the collection of information is estimated to average 1 hour per response, including the time for reviewing instructions, searching existing data sources, gathering and maintaining the data needed, and completing and reviewing the collection of information. Send comments regarding this burden estimate or any other aspect of this collection of information, including suggestions for reducing this burden, to Washington Headquarters Services, Directorate for Information Operations and Reports, 1215 Jefferson Davis Highway, Suite 1204, Arlington VA 22202-4302. Respondents should be aware that notwithstanding any other provision of law, no person shall be subject to a penalty for failing to comply with a collection of information if it does not display a currently valid OMB control number.

1. REPORT DATE	2. REPORT TYPE	3. DATES COVERED
MAY 1980		**00-00-1980 to 00-00-1980**

4. TITLE AND SUBTITLE	5a. CONTRACT NUMBER
Molecular Dynamics Simulation Studies of Fracture in Two Dimensions	5b. GRANT NUMBER
	5c. PROGRAM ELEMENT NUMBER
6. AUTHOR(S)	5d. PROJECT NUMBER
	5e. TASK NUMBER
	5f. WORK UNIT NUMBER
7. PERFORMING ORGANIZATION NAME(S) AND ADDRESS(ES) **Massachusetts Institute of Technology,77 Massachusetts Avenue,Cambridge,MA,02139-4307**	8. PERFORMING ORGANIZATION REPORT NUMBER
9. SPONSORING/MONITORING AGENCY NAME(S) AND ADDRESS(ES)	10. SPONSOR/MONITOR'S ACRONYM(S)
	11. SPONSOR/MONITOR'S REPORT NUMBER(S)

12. DISTRIBUTION/AVAILABILITY STATEMENT
Approved for public release; distribution unlimited

13. SUPPLEMENTARY NOTES

14. ABSTRACT

Computer Molecular Dynamics (CMD) simulation has been applied to the study of fracture in a two-dimensional system. The system was composed of an atomic crack tip embedded in an infinite continuum medium under an external tensilestress (mode-I fracture). The structure and properties of the crack tip have been analyzed for materials characterized by several types of interatomic potential functions. This technique provides a unique way of investigating the non-linear atomic effects around the crack tip. A computer program has been developed which can be applied to any system of classical particles, crystalline solids, liquids or gases, under a wide range of boundary conditions, periodic, free, fixed and flexible boundaries. In particular, two kinds of boundary conditions have been employed in the study of the crack tip structure and stability in a two-dimensional triangular lattice. One is a fixed boundary condition which consists of fixing the particles at the boundaries according to a continuum elasticity solution and relaxing the system by introducing a viscous damping in the equations of motion. The second procedure is a flexible boundary condition which treats the simulation region as a discrete system embedded in a continuum. A linear Green's function is used to relax the forces arising from interactions between the atomic region and the continuum. This method is shown to be efficient and accurate in the determination of crack configurations in brittle materials. It is potentially useful for the study of other defect properties. The critical stress necessary to propagate a crack of finite length has been determined in the case of brittle materials. Higher values than those predicted by the Griffith theory have been obtained. The results seem to be very sensitive to the assumptions about interactions between the crack surfaces. Plasticity around the crack tip was also studied. Several atomistic processes of plastic relaxation produced by simultaneous shear and rotation of the lattice were observed and the rotation and strain fields around the crack tip calculated. The Kelly, Tyson and Cottrell (KTC) and Rice-Thomson (RT) criteria for predicting brittle or ductile behavior were studied and their predictions compared to CMD observations. KTC criterion seems to agree well with CMD results whereas the RT criterion underestimates the possibility of ductile behavior.

15. SUBJECT TERMS

16. SECURITY CLASSIFICATION OF:			17. LIMITATION OF ABSTRACT	18. NUMBER OF PAGES	19a. NAME OF RESPONSIBLE PERSON
a. REPORT	b. ABSTRACT	c. THIS PAGE			
unclassified	**unclassified**	**unclassified**	**Same as Report (SAR)**	**126**	

MOLECULAR DYNAMICS SIMULATION STUDIES OF FRACTURE IN TWO DIMENSIONS

by

BENITO de CELIS

Submitted to the Department of Nuclear Engineering
on May 30, 1980 in partial fulfillment of the
requirements for the degrees of
Nuclear Engineer and Master of Science

ABSTRACT

Computer Molecular Dynamics (CMD) simulation has been applied to the study of fracture in a two-dimensional system. The system was composed of an atomic crack tip embedded in an infinite continuum medium under an external tensile stress (mode-I fracture). The structure and properties of the crack tip have been analyzed for materials characterized by several types of interatomic potential functions. This technique provides a unique way of investigating the non-linear atomic effects around the crack tip.

A computer program has been developed which can be applied to any system of classical particles, crystalline solids, liquids or gases, under a wide range of boundary conditions, periodic, free, fixed and flexible boundaries. In particular, two kinds of boundary conditions have been employed in the study of the crack tip structure and stability in a two-dimensional triangular lattice. One is a fixed boundary condition which consists of fixing the particles at the boundaries according to a continuum elasticity solution and relaxing the system by introducing a viscous damping in the equations of motion. The second procedure is a flexible boundary condition which treats the simulation region as a discrete system embedded in a continuum. A linear Green's function is used to relax the forces arising from interactions between the atomic region and the continuum. This method is shown to be efficient and accurate in the determination of crack configurations in brittle materials. It is potentially useful for the study of other defect properties.

The critical stress necessary to propagate a crack of finite length has been determined in the case of brittle materials. Higher values than those predicted by the Griffith theory have been obtained. The results seem to be very sensitive to the assumptions about interactions between the crack surfaces. Plasticity around the crack tip was also studied. Several atomistic processes of plastic relaxation produced by simultaneous shear and rotation of the lattice were observed, and the rotation and strain fields around the crack tip

calculated. The Kelly, Tyson and Cottrell (KTC) and Rice-Thomson (RT) criteria for predicting brittle or ductile behavior were studied and their predictions compared to CMD observations. KTC criterion seems to agree well with CMD results whereas the RT criterion underestimates the possibility of ductile behavior.

Thesis Supervisor:	Sidney Yip
Title:	Professor of Nuclear Engineering
Thesis Co-Supervisor:	Ali Argon
Title:	Professor of Mechanical Engineering

Acknowledgements

I would like to express my sincere gratitude to Professor Sidney Yip for his guidance, encouragement and support throughout this work. I am equally indebted to Professor Ali Argon for his invaluable assistance in the problems associated with fracture mechanics.

I also wish to thank the Instituto Technologico para Postgraduados (Spain) and the Army Research Office, Contract DAAG-29-78-C-0006, for financial support.

Table of Contents

List of Figures

List of Tables

Chapter One

Introduction

1. Introduction

Computer molecular dynamics (CMD) is a powerful technique for calculating equilibrium and dynamical properties of solids. The method consists of calculating the classical trajectories of several hundreds of particles interacting through a known potential function, by numerical integration of the equations of motion.

The equations of motion which govern the time evolution of the nuclear coordinates are a set of coupled, non-linear ordinary differential equations. The time evolution of the phase coordinates is called the trajectory, and the CMD technique consists of numerically integrating the equations of motion to solve for the trajectory at discrete time points. The classical statistical mechanics relates thermodynamic properties to the average value of functions of the phase coordinates of the atoms. The average is usually taken over all elements of the ensemble which corresponds to a given macrostate.

The present work is a study of the static properties of fracture in crystalline solids. Using CMD simulation results, a number of continuum theory predictions are tested at an atomic level, and the effects of non-linear relaxation observed.

It is well known that to find a general solution to the static configuration around defects of irregular geometries can be a difficult task even in the approximation of a linear theory. Moreover, there are cases where the system behavior is determined by a region that is only a few interatomic spacings in extent; then non-linear atomistic processes can not be ignored. In such cases CMD can be an extraordinarily useful technique for studying the static configuration of the defect as well as its dynamic properties.

The first studies of fracture in a discrete lattice were carried out with very simple models in one or two dimensions and highly idealized interatomic force laws.[1] These simplified models, however, contributed greatly to the understanding of the macroscopic properties of fracture, such as brittle versus ductile behavior, and determination of elastic constants, ideal maximum cohesive and shear stress, etc., in terms of microscopic physical variables, such as lattice structure, interatomic force law, etc.

Subsequent studies using computer simulation were concerned with systems of larger number of particles and more realistic interatomic force laws, such as the calculations for iron by Kanninen and Gehlen[2] and for silicon by Sinclair and Lawn.[3]

The main difficulty with these computer simulations has been the specifications of the external boundary conditions. Periodic boundary conditions is a simple and accurate way of simulating the properties of an infinite homogeneous system. However, when the system is acting under the effect of an external force, a different procedure must be used. One alternative is to apply the external forces directly over the free surfaces of the system. The other consists of matching the solution at the boundaries to a continuum elasticity solution. Of the two alternatives, only the second has a practical application in the study of a macroscopic crack under the action of an exterior stress applied far from the crack and it alone will be used in our simulations.

Dynamics of crack propagation has been studied by computer molecular dynamics by Sander,[4] by Weiner and Pear[5] and by Ashurst

and Hoover.[6] All these studies show the influence of atomic structure and interatomic force laws on the dynamics of crack propagation. These simulations used free boundaries and the stresses were applied directly over the exterior atoms, close to the crack tip. It was found that the results differ substantially from predictions given by macroscopic theories, and it seems appropriate to consider more realistic border conditions if one wants to simulate the behavior of cracks in real materials or establish a direct comparison between continuum and atomistic results.

Our study of static properties of fracture by CMD consists of simulating the crack tip behavior in a two-dimensional atomic system, introduced in an infinite continuum medium under the action of an external stress (mode-I fracture).

The static equilibrium configuration of the system is obtained by applying a frictional damping to the equations of motion. The general techniques used in this work jointly with the standard methods of CMD are summarized in Chapter Two, where a description of the problems associated with the different types of boundary conditions is also included.

Chapter Three summarizes several important concepts in continuum theory of fracture, namely, the Griffith's theory of brittle materials, and the criteria which have been recently developed to predict brittle or ductile behavior in crystalline materials. The last section of this chapter describes previous research done in this area by CMD.

The description of the technique used in this work, flexible boundary, is done in Chapter Four, jointly with the method to determine the elastic constants, ideal stresses and surface energy of a material whose atoms interact through a known pair potential function. These physical constants are important not only for calculating the displacement field according to linear continuum solutions, but also for predicting brittle or ductile behavior of the system. In the last part of the chapter the critical stress to propagate a crack in a given material is determined by direct application of the flexible boundary technique and these results are compared with continuum linear elasticity theory.

Plasticity around the crack tip has been studied in Chapter Five. Two criteria to determine brittle or ductile behavior of a given material, one due to Kelly, Tyson and Cottrell (KTC) and another due to Rice and Thomson (RT), are studied and their predictions compared to CMD simulations.

Emission of dislocations and several microscopic processes of plastic deformation have been observed in the simulation results. The strain and rotation fields around the crack tip for several potential functions have been determined. Finally, a summary with conclusions, discussion of results, and suggestions of further work are given in Chapter Six.

Chapter Two

Computer Molecular Dynamics Techniques

2.1 Equations of Motion

In CMD calculations, a three-dimensional system of N particles is treated by setting up 3 N classical equations of motion which are coupled through an assumed two-body interaction potential. This set of 3 N simultaneous differential equations is then integrated numerically on a computer to give the spatial trajectories and velocities of all the particles as a function of time.

In the present simulation, a classical system of N point particles of mass m is assumed to obey Newtonian mechanics, in which case the equations of motion are given by

$$\frac{d^2\vec{r}_i}{dt^2} = \frac{1}{m}\vec{F}_i(\vec{r}_1, \vec{r}_2, \ldots \vec{r}_n) + \frac{\vec{F}_i^{ext}}{m}; \; i=1,2,\ldots N \qquad (2\text{-}1)$$

where $\vec{r}_i$ is the portion coordinate of the ith particle, $\vec{F}_i$ and $\vec{F}_i^{ext}$ are the vector forces on the ith particle due to other particles and exterior force respectively. For central, conservative, pairwise additive potentials, the pair force F_{ij} between two particles i and j of the system is the gradient of $\phi(r_{ij})$ with respect to $\vec{r}_{ij}$, i.e.,

$$\vec{F}_{ij}(\vec{r}_{ij}) = -\frac{\partial \phi(r_{ij})}{\partial \vec{r}_{ij}} \qquad (2\text{-}2)$$

where $\phi(r_{ij})$ is the pairwise potential between the particles i and j. It is a function of the pair separation vector r_{ij} between these two particles.

2.2 Potential Function

Empirical and semi-empirical potential functions can be constructed in which adjustable parameters are determined by matching certain calculated properties of the system to experimental results. Two fundamental assumptions are almost universally employed: central forces and pairwise additivity. Pairwise additivity means that the potential energy between two atoms is unaffected by the presence of other nearby atoms. The central force assumption means that the force between atoms is directed along the line joining the centers of mass and so is a function only of the atomic separation. The next discussion goes into commonly known empirical and theoretical potential functions which have been used in our computer simulations.

Some interatomic potentials are characterized by a single functional form which varies continuously over the entire range of interatomic spacing and has short range repulsive and long range attractive forces. A potential of this kind was employed by Lennard-Jones[1] in which the attractive and repulsive parts vary as the inverse of the 12 and 6 power, respectively. This potential has often been used to represent the effective pair interactions in rare gases and in simple non-polar molecules as N_2 and CH_4:

$$\phi(r) = 4\varepsilon \left\{ \left(\frac{\sigma}{r}\right)^{12} - \left(\frac{\sigma}{r}\right)^{6} \right\} \qquad (2-3)$$

This potential gives qualitative agreement with rare gas properties in condensed phases and is computationally convenient because the entire potential is expressed in pairwise additive two-body terms.

A form extensively used for metals is the Morse[2] potential

$$\phi(r) = D\left\{ e^{-2\alpha(r-r_0)} - 2\, e^{-\alpha(r-r_0)} \right\} \qquad (2-4)$$

where α and D are constants with dimensions of reciprocal distance and energy, respectively, and r_0 is the equilibrium distance corresponding to the minimum of the potential. The Morse potential approaches zero exponentially at large distance, in accord with the Thomas-Fermi model of electronic screening. It also yields an exactly soluble Shrodinger equation for the vibrational eigenvalue problem of diatomic molecules and the eigenvalue distribution is in good agreement with experimental spectroscopic measurement.[2]

The most important characteristics of this potential pertaining to our CMD simulation of fracture is that the three parameters D, α and r_0 of the potential for several f.c.c. and b.c.c. metals have been determined using experimental values for the energy of vaporization, the lattice constant, and the compressibility.[3]

The estimates of the validity of the Morse potential in metals given in the preceding paragraphs apply to a perfect crystal. An additional complication is introduced if defects are present. The Morse potential constants computed from the energy of vaporization, the lattice constant, and the compressibility refer to a perfect lattice and reflect its electronic distribution. The presence of a defect, however, alters the electron distribution, and it is difficult to estimate how this altered distribution would affect the atoms in the vicinity of the defect.[3]

2.3 Numerical Integration of Equation of Motion

The algorithm used to move the particles forward in time by an amount Δt is given by

$$r(t+\Delta t) = r(t) + v(t)\Delta t + \frac{1}{6}\left[4a(t) - a(t-\Delta t)\right]\Delta t^2 \qquad (2\text{-}5)$$

$$v(t+\Delta t) = v(t) + \frac{1}{6}\left[2a(t+\Delta t) + 5a(t) - a(t-\Delta t)\right]\Delta t$$

where r(t), v(t) and a(t) are the position, velocity and acceleration of a particle at time t. This algorithm, used by P. Shofield in CMD simulation of liquids[4] is very strongly conserving and allows a relatively large time step to be used.

We have checked the accuracy of this algorithm by comparing it with the exact solution for the harmonic oscillator. Both solutions, the exact and the approximation, have been expanded in powers of t.

(a) Exact solution corresponding to an harmonic oscillator

$$x(t) = x(0) + \frac{v(0)}{\omega}\sin(\omega t) \qquad v(t) = v(0)\cos(\omega t)$$

Substituting t by $t + \Delta t$ in the above equations and expanding $\sin(\omega(t+\Delta t))$ and $\cos(\omega(t+\Delta t))$

$$x(t+\Delta t) = x(t) + v(t)\Delta t + \frac{\Delta t^2}{2}a(t) - \frac{v(t)\omega^2\Delta t^3}{3!} + \frac{v_0}{\omega}\frac{\sin\omega t(\omega^4\Delta t^4)}{4!} + \cdots \qquad (2\text{-}6)$$

$$v(t+\Delta t) = v(t) + a(t)\Delta t + v_0\cos\omega t\left(\frac{-\omega^2\Delta t^2}{2!}\right) + v_0\cos\omega t\left(\frac{\omega^3\Delta t^3}{3!}\right) + v_0\frac{\cos\omega t(\omega^4\Delta t^4)}{4!} + \cdots$$

(b) Algorithm (2-5), expanded in powers of Δt

$$x(t+\Delta t) = x(t) + v(t)\Delta t + \frac{\Delta t^2 a(t)}{2} - \frac{v(t)\omega^2\Delta t^3}{3!} - \frac{v_0}{\omega}\frac{\sin(\omega t)\,\omega^4\Delta t^4}{12} + \ldots \qquad (2\text{-}7)$$

$$v(t+\Delta t) = v(t) + a(t)\Delta t + v_0\cos\omega t\left(-\frac{\omega^2\Delta t^2}{2!}\right) + \frac{v_0\sin(\omega t)\,\omega^3\Delta t^3}{12} + \ldots$$

Equation (2-7) shows that the algorithm used by Schoefield is correct to order $(\Delta t)^3$ and $(\Delta t)^2$ for the positions and velocities, respectively, when it is tested against the harmonic oscillator solution.

This algorithm has the advantage that it needs less terms to calculate $r(t+\Delta t)$ and $v(t+\Delta t)$ in expression (2-5) than the ordinary central difference method for the same order of accuracy and the disadvantage that the evaluation at time $t+\Delta t$ is carried out using the values at t and $t-\Delta t$, therefore a different procedure is needed to initialize the numerical integration at time $t = 0$.

2.4 Accuracy of Numerical Integration: Conservation of Energy and Reversibility of Trajectories

The time step size has to be chosen small enough that the integration procedure generates a stable solution to the equations of motion. If the time step size is too large, then the equations of motion will fail to conserve total energy and will result in an unstable phase space trajectory. On the other hand, it also has to be chosen as large as possible because the computational time per time step does not depend on the time step size, and the net cost of a simulation over a fixed duration will vary inversely as the time step

size. The numerical integration should also span an oscillation period in a number of time steps, i.e., ~10, such that the net change during any single time step is not too large. The accuracy of the numerical integration can be measured by the precision to which the total energy is conserved. A series of simulations with different time step sizes at different temperatures was carried out on a perfect lattice composed of 64 particles to determine the maximum time step size that gave reasonable conservation in the total energy. Time step sizes as large as 1/10 of an oscillation period gave absolute deviations of about 0.05% per time step, and were considered acceptable. However, more conservative time step sizes, about 1/50 of one oscillation period, were used.

The accuracy of the numerical integration can also be measured by the accuracy of the reversibility of trajectory. The trajectory can be retraced simply by reversing velocities and other odd time derivations at the time step of retracing or well by using a negative value for Δt at every time step. The accumulated error in the total energy during a computation period of one thousand time steps (500 time steps before reversing trajectories), at a temperature of 60°K, was less than 2%.

2.5 Potential Range Cut-off

The number of neighbors that are included in a CMD simulation is an important parameter because the calculation time scales linearly with the total number of interacting neighbors. The total number depends on the potential cut-off or the distance at which the force becomes negligible by comparison with the force between nearest neighbors.

However, the elimination of direct interaction between a pair of particles separated by other interacting particles does not preclude indirect communication between those particles. Each particle in the system is dynamically coupled to every other particle in the system either directly or indirectly.

In the simulation of fracture the cut-off range plays an important role because the propagation of the crack is produced by bond rupture in tension when they reach the cut-off range, or by bond rupture in shear in which case the crack is blunted. The surface energy is another parameter that can change significantly if an appropriate cut-off range is not chosen. We have chosen in our simulations only first nearest neighbor interaction with the potential function truncated at a distance where the force can be neglected. Besides, several tests were done using second nearest neighbors and the results did not change significantly.

2.6 Boundary Conditions

The behavior of an infinite system is approximated by describing the motion of N particles in a finite computational cell of volume V with periodic boundary conditions.

If one wants to use this procedure to study the behavior of defects, the system must be large enough such that the images do not interact with the original defect. An additional difficulty arises when the defect is subject to a certain state of stress. Then, the position of the particles must be generated according to some known theory specifying that state before periodic boundary conditions can be applied.

To overcome these difficulties in the simulation of fracture, two general procedures have been implemented during the last few years. One consists of generating the state of stress by applying forces directly over the free boundaries of the system with the defect. The disadvantage of using this procedure is that it is very expensive to work with a system large enough to avoid interactions between boundaries and the defect. The other method arranges the atoms at the boundaries according to the solution given by the linear elasticity theory and studies the behavior within the system, where linear elasticity theory is in general not valid, using computer molecular dynamics.

The last procedure which is the one used in this work has the great advantage of reproducing exactly the macroscopic conditions with a relatively small number of particles letting exact calculations of the defect structure. This procedure is called fixed boundary condition.

A further improvement appears when it is found that after the relaxation of the atomic non-linear region using CMD, small residual forces arise at the boundaries due to the difficulties of the continuum linear solution applied at the boundaries to accomodate the atomic region after the relaxation. In this case, what has been recently applied is a continuum linear Green's function, which gives the displacement field due to a unit force at some distance from the crack necessary to cancel the small remaining forces.

This method called flexible boundary has been applied in this work to determine crack tip configuration and the critical stress

intensity factor of brittle materials. In a few cases where it was found a large plastic region, formed by emission of dislocations from the crack tip, the first steps of the technique, which constitutes the fixed boundary method, was applied to a large system to avoid the interaction of the extending plastic region with the boundaries.

2.7 Determination of Equilibrium Configuration

Several different kinds of computer experiment methods can be used to obtain the defect configuration. They are classified, according to Beeler,[5] in five types: dynamical, frictional damping, variational, Monte-Carlo and lattice-static methods. A pairwise atomic interaction model is assumed for computing structure-dependent forces and energy contributions. Structure independent forces and their associated energy contribution usually are accounted for by specification of appropriate boundary forces and the atomic volume. Detailed descriptions of the first four methods and their applications are given in Ref. 6. The lattice-static method is explained in Refs. 7 - 9.

In the dynamical simulation of a crystal, each atom vibrates continuously about its static equilibrium position. The array of atomic positions can be obtained by computing the time-average portion of each atom. In instances where only the time-average portions are desired, the dynamical method can be amended so that the atom motion is progressively damped as the atoms approach their static equilibrium portions.

There are several procedures for reaching the static equilibrium configuration. Gibson et al.[10] introduced a frictional method for

static equilibrium configuration calculations wherein the velocity of each atom is set to zero each time the kinetic energy of the entire system reaches a maximum. This procedure is suggested by the circumstance that the velocity magnitude of a mass point in simple harmonic motion is maximum at the time it is passing through the static equilibrium position (zero net force position). Several variations of this basic idea have evolved. As a mass point, in simple harmonic motion, approaches the static equilibrium position, the dot product of its velocity and the restoring force in a monotomically decreasing positive quantity which vanishes at the equilibrium position and then becomes negative. On this basis, Evans and Beeler introduced the idea of setting the velocity of any atom to zero whenever the velocity-force dot product becomes negative, in a static equilibrium calculation. This individual atom criterion for damping leads to a significantly faster convergence than the maximum total kinetic energy criterion.

The procedure used in this work consists of introducing a frictional force in the equations of motion of each particle after the system has released freely for several oscillations of the total kinetic energy:

$$m \frac{d^2 \vec{r}_i}{dt^2} = \vec{F}_i (\vec{r}_1 , \vec{r}_2 , \ldots , \vec{r}_N) - \alpha \frac{d \vec{r}_i}{dt} \qquad (2\text{-}8)$$

The damping constant has to be chosen small enough that the system is not so overdamped that it is quenched, and as large as possible so the system will reach the minimum internal energy configuration

in a reasonable period of time. Usually the damping constant is chosen to be around half the time average value of the critical damping constant estimated by Hooke's Law. We did several tests with different damping constants and found that for values close to the critical damping, the average time for the system to reach the minimum internal energy configuration was about 300 time steps. The total procedure, therefore, consists of several periods of free relaxation alternating with periods with frictional damping until the system temperature has decreased to a few degrees Kelvin. The final configuration corresponds to a stable state of minimum potential energy and further damping to still lower temperatures does not lead to any significant different configuration of the relaxed atomic positions.

Chapter Three

Computer Molecular Dynamic Simulation of Fracture

The following sections are devoted to summarize some of the general concepts and theories of macroscopic fracture mechanics which will be examined, from an atomistic point of view, in the present work. A description of the different models and recent results in atomic simulation of fracture is given in Section 3.3 of this chapter.

3.1 Griffith Theory of Brittle Materials

Griffith's idea was to set up a model for a crack system in terms of a reversible thermodynamical process.[1,2] The important elements of the system are defined in Fig. 3.1: an elastic body B containing an internal crack S of length 2C is subjected to loads applied at the outer boundary L.

The first step in the treatment was to find an expression for the total energy of the system. To do this the individual energy terms which change as a result of crack formation are considered. First, it can be expected in general that the outer boundary of the cracked body will undergo some displacement, such that the applied load does an amount of work W_L. (For a truly reversible system an increase in this work can be identified with a corresponding decrease in the potential energy of the loading system.) Second, the strain energy V_E stored in the elastic medium must be sensitive to any variations in the system geometry. Third, the mere act of creating new crack surfaces requires the expenditure of free surface energy V_S. For a static crack system the total energy is the sum of threse three terms:

$$V = (-W_L + V_E) + V_S \qquad (3.1)$$

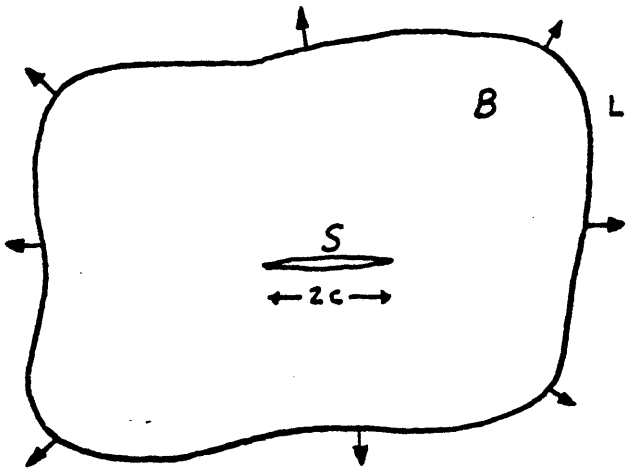

Figure 3.1 Static plane crack system. L applied loading, S crack surface.

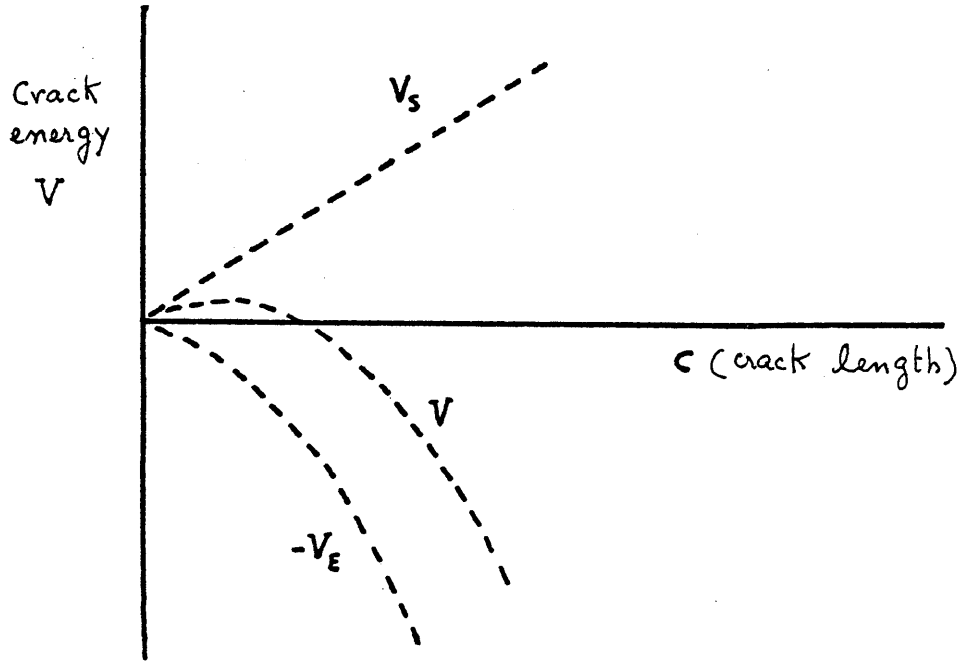

Figure 3.2 Energetics of Griffith crack in uniform tension.

Since forces transmitted to the crack region are determined by the loading system and elastic medium, it is convenient to refer to the bracket term in Eq. (3-1) as the mechanical energy of the system. Of course, if we were to be concerned with a dynamic crack system, we would have to add a kinetic energy term to Eq. (3-1).

Thermodynamic equilibrium is then attained by balancing the mechanical and surface energy terms over a virtual crack extension . The mechanical energy must decrease as the crack extends. On the other hand, the surface energy term must increase with crack extension, since the cohesive forces of molecular attraction across δc must be overcome during the creation of the new fracture surfaces. Thus, the bracket term in Eq. (3-1) favors crack extension, while the second opposes it. This is the Griffith energy balance concept, a formal statement of which is given by the extended equilibrium requirement

$$\frac{dV}{dc} = 0 \qquad (3-2)$$

Griffith attempted to confirm his theory by applying it to a real situation. He needed a model for a crack in order to calculate the energy terms in Eq. (3-1). For this he took advantage of the Inglis analysis,[3] considering the case of a narrow elliptical crack in a remote, uniform tensile stress field. Then, for experimental verification he had to find a well behaved, model material, isotropic and closely obeying Hooke's law at all stress levels prior to fracture. Glass was selected as the most easily accessible material satisfying these demands.

In evaluating the mechanical energy of his model, Griffith used a result from linear elasticity theory, namely that for any body under constant applied stress during crack formation,

$$W_L = 2 V_E \quad (\text{constant stress}) \qquad (3\cdot 3)$$

From the Inglis solution of the stress and strain fields, the strain energy density is readily computed for each volume element about the crack. Integrating over dimensions large compared with the length of the crack then gives, for unit width of the crack (measured along the crack front[3,4]

$$V_E = \pi C^2 \sigma_L^2 / E \quad (\text{plane stress}) \qquad (3\cdot 4a)$$

for a thin plate, or

$$V_E = \pi (1-\nu^2) C^2 \sigma_L^2 / E \quad (\text{plane strain}) \qquad (3\cdot 4b)$$

for a thick plate. Here σ_L is the applied tension normal to the crack plane, E is Young's modulus, ν is Poisson's ratio, and 2C is the length of the crack. The application of additional loading parallel to the crack plane has negligible effect on the strain energy term in Eq. (3-4). For the surface energy of the crack system, Griffith wrote for unit width of crack

$$V_S = 4 C \gamma \qquad (3\cdot 5)$$

with γ the free surface energy per unit area. The total system energy Eq. (3-1) thus becomes for the case of plane stress

$$V = -\pi c^2 \sigma_L^2 / E + 4c\gamma \qquad (3-6)$$

The Griffith equilibrium condition, Eq. (3-2), may now be applied to Eq. (3-6); this gives as a critical condition for fracture

$$\sigma = (2E\gamma / \pi c)^{1/2} \qquad (3-7)$$

for constant stress, plane stress conditions (Fig. 3.2).

In the above case, the analysis has been applied to a crack in a brittle elastic solid where its movement does not involve plastic deformation. It is significant that the same approach can also be applied to problems where the movement of the crack involves plastic deformation with the assumption that the plastic region around the crack tip is negligibly small in comparison with the outer zone (Irving approach). In this case we may substitute γ by γ_p, where γ_p is the plastic work done in forming a square centimeter of surface. Under these circumstances the γ surface, defined in terms of the energy to break atomic bonds must include the energy due to all the mechanism of plastic relaxation produced during the crack extension.

3.2 Brittleness and Ductility of Crystalline Materials

There is extensive literature covering all the continuum and atomistic aspects of crack tip plasticity. In this section a model of dislocation nucleation at the tips of cracks and the influence of

such defects to predict brittle or ductile behavior as described by Kelly, Tyson and Cottrell (KTC)[5] and by Rice and Thomson (RT)[6] is discussed.

A criterion for brittle fracture in crystals can be established in terms of the spontaneous emission of dislocations from a sharp crack. The stress field near the crack tip in a linearly elastic medium is of the form $\sigma_{ij} = K(2\pi r)^{-1/2} f_{ij}(\theta)$ where K is the stress intensity factor and (r,θ) are polar coordinates with the origin at the crack tip. At the crack tip itself where $r \to 0$ a non-linear treatment is required as the interatomic bonds are stretched beyond the region of harmonic behavior. As the stress intensity increases, lattice failure will occur at the crack tip in the non-linear region. Failure can occur by bond rupture in either tension or shear, which will determine whether the behavior is inherently brittle or ductile.

Two treatments have been presented in the literature to predict the failure mode from known material properties. Kelly, Tyson and Cottrell proposed the criterion that an ideal (defect-free) solid may sustain a fully brittle crack only if the theoretical strength in tension is exceeded before the theoretical strength in shear within the local field of the tip. The criterion makes no comment on the nature of any shear deformation that might happen. One only needs to consider the theoretical strength calculations in relation to the stress distribution at the crack tip, coming back to the equations of linear elasticity for an evaluation of this field. The final expression proposed by KTC was that brittle fracture would be observed if $\left(\sigma_{SHEAR} / \sigma_{COHESIVE}\right)_{ideal} > \left(\sigma_{SHEAR} / \sigma_{COHESIVE}\right)_{max}$ where the subscripts "ideal" and "max"

refer to the ideal properties of a perfect lattice and to the maximum values attained at a crack tip respectively.

Rice and Thomson[6] on the other hand, have argued that a necessary criteron for brittle fracture is stability against the emission of dislocations from the crack tip. They have treated this nucleation process within the approximation of linear elasticity and the Peierls model of a dislocation core. the specific question addressed by these workers is whether the shear deformation is sufficient, not merely to nucleate a dislocation at the crack tip, but also to propagate it within the stress field into the surrounding crystal. They considered first the balance between the following crack-dislocation interaction forces: (a) force on dislocation arising from stress field of crack, (b) surface tension force caused by creating surface ledges at (blunted) crack, (c) image force of dislocation in the free surface of crack. The first term repels the dislocation from the crack tip, while the remaining two attract it. One then compares the cores of the dislocation versus the distance in which the dislocation starts to be repelled from the crack tip.

Rice and Thomson thus conclude that covalent and ionic solids, along with h.c.p. metals, are stable against dislocation emission, while f.c.c. metals are unstable; b.c.c metals comprise an intermediate case. The KTC criterion probably leads to an underestimate of the brittle tendencies of the solids because of not considering the subsequent propagation of newly generated shear deformation (dislocation).

Both treatments require approximations in their quantitative development. The stress analysis of linear elasticity is used to evaluate $\left(\sigma_{SHEAR} / \sigma_{COHESIVE}\right)_{max}$ around the crack tip in the KTC criterion and the forces on dislocations near the crack tip in the RT model. Better models of the non-linear and atomistic behavior of materials are also required to evaluate $\left(\sigma_{SHEAR} / \sigma_{COHESIVE}\right)_{ideal}$ and dislocation core structure with greater accuracy.

3.3 Computer Molecular Dynamics of Fracture - Previous Works

During the last years a number of studies of fracture in crystalline solids using atomistic models have appeared. One can classify them in two categories. The first type is concerned with a specific material or group of materials, and its purpose is to be as realistic as possible with respect to both crystal geometry (dimensionality of the system, boundary conditions, etc.) and interatomic force laws. These models must yield information regarding atomic processes in the given class of materials. Examples are provided by the work of Kanninen and Gehlen[7,8,9] and Sinclair.[10]

Gehlen and Kanninen worked on α-iron in a three-dimensional lattice on which the atoms interact through a central pair potential constructed by Johnson. This potential is based upon two-body interactions which extend out to first and second nearest neighbors. An empirical form is used with the constants selected to match the experimentally determined elastic constants of the material. The atoms are initially put into a configuration approximating the defect being simulated. The boundary atoms are held fixed in the positions given by the linear elastic continuum solution (fixed boundary condition).

The final position of atomic equilibrium is evaluated by letting the atoms inside the system move freely according to the interatomic forces.

Based on this model Gehlen and Kanninen tried to check the validity of Griffith's criterion. All the macroscopic variables, elastic constants and surface energy were specified by the potential function and the critical stress was determined by calculating the condition of maximum elongation for the crack tip bond. The estimated values for the critical stress intensity factor were found to be greater than those necessary to produce an exact correspondence with Griffith's equation. A possible reason for this discrepancy, as noted by the authors, is that the boundaries were fixed. This inflexibility could produce high residual forces between the atomic and continuum regions, especially if the atomic boundaries are close to the crack tip. To avoid these difficulties the authors used a new procedure called flexible boundary to attenuate the effects of the lack of adjustment between the two regions. In the present work an improvement of this method is applied to crack tips and it will be discussed in Chapter Four.

The second type of atomistic models is highly idealized from the viewpoint of crystal geometry (two dimensions, free boundaries, etc.) and interatomic force laws. They cannot, therefore, represent directly any particular real material. Nevertheless, they do serve to provide insight into general characteristics of static and dynamic propagation of crack with a minimum of computational difficulties. Examples of idealized atomistic models include the works of Thomson,

Hsieh and Rana[11,12,13] in which a new phenomenon called "lattice trapping", the crack analogy of the Peierls resistance to a dislocation motion, is studied. They used two models which were subjected to a "lattice-static" analysis. In the first model, a one-dimensional system, the crack was depicted as two semi-infinite chains consisting of points of atoms linked horizontally by bendable elements and vertically by stretchable elements. The chains were subjected to opening forces applied vertically at the free ends. In the two-dimensional model an infinite square lattice of atoms linked by stretchable and bendable elements was considered. The crack was opened either by a vertical wedging force or by vertical tensile forces distributed uniformly at infinity. The "lattice-static" analysis began with an assumption concerning the form of the atomic interaction, and proceeded to calculate an equilibrium configuration consistent with appropriate boundary conditions. This involved considerable mathematical complexity, and one had to restrict the analysis to the simplest force laws for the linking elements. Accordingly it was assumed that the elements were Hookean up to a critical breaking point. The lattice trapping behavior has been tested with other atomistic models, using CMD, by P.C. Gehlen and M.F. Kanninen,[9] and A. Gohar.[14] These results seemed to indicate that the phenomenon of lattice trapping is almost completely attenuated when more realistic interatomic force laws are used in the simulation.

Highly idealized modes have been used in the studies of Ashurst and Hoover[15] and Weiner and Pear.[16] Ashurst and Hoover used a two-dimensional triangular lattice in which the particles interact by

truncated Hooke's law forces and the exterior stresses acted directly over the free boundaries. Their static results for the energy, entropy, stress concentration and crack structure are consistent with expectations from macroscopic elasticity theory. The dynamic theory of crack propagation is, according to the authors, less well developed and supersonic crack velocities could be produced by the proximity of the exterior boundaries. Under these conditions crack propagation can outrun lattice relaxation. These effects can be avoided if the crack is enclosed in a continuum elastic medium in which the stresses are acting at infinity. Then the crack propagation will be only affected by the natural relaxation of the strain field around the crack and will not be influenced by the proximity of the exterior boundaries. This second model is more realistic but it introduces additional computational difficulties that remain to be solved. In the next chapter we give a full description of the advantages and limitations of this method, called flexible boundary conditions.

Chapter Four

Flexible Boundary Conditions

4.1 Description

Several kinds of boundary conditions have been applied recently to the study of crack tip configurations. Some of them, periodic boundaries, free boundaries with stresses applied directly on the free surface, etc., were summarized in Chapter Three. In this section we give a complete description of the so-called flexible boundary (FB) developed by Sinclair et al.[1] The next section describes the determination of elastic constants for a two-dimensional triangular lattice, a step that is necessary in applying the continuum elasticity solutions at several stages of FB.

Several methods of flexible boundary[2,3] have been developed. They differ only in the way the atomic forces arising from the interaction of the continuum with the atomic region are relaxed. These techniques, as noted by Sinclair et al,[1] have improved the efficiency of the calculations by permitting the use of smaller atomic systems, have yielded descriptions of the dilatational effects arising from non-linearity in the core of the defect, have allowed equilibrium to be established between the atomic and continuum regions, and have made possible calculations of defect mobility by removing the constraints imposed by rigid boundaries.[2-6]

The first step in imposing FB begins with a perfect lattice of the type of material which is going to be studied. The first configuration of the defect is then generated with all the atoms in the system displaced according to a linear continuum solution. This solution gives the displacement field under fixed conditions (type of stress boundary conditions, etc.) and the core of the defect is arbitrarily

fixed at the center of our system. The resulting array is then divided into three regions as shown in Fig. 4-1 for the case of a crack tip. Region-I contains those atoms which are going to be moved according to CMD, under the force law of a chosen two-body central potential. Region-II is composed of atoms which interact with atoms in Region-I or Region-III, and contains all the atoms on which a force may be exerted by at least one atom in Region-I. The thickness of Region-II should thus equal the maximum range of the interatomic force law. Region-III is composed of the exterior atoms which are always displaced according to a linear continuum solution. The thickness of Region-III should correspond to the minimum distance to completely determine the forces acting on each Region-II atom and is also equal to the maximum range of the potential function.

The second step is to relax Region-I atoms using CMD. Several alternative procedures can be used to reach a relaxed configuration in which the forces on the Region-I atoms are less than a predetermined value. The procedure followed here has been explained in Chapter Two; it is a method which continuously takes out kinetic energy from the system through a frictional force.

The third step uses the residual forces acting on Region-II atoms, generated by the relaxation of Region-I, to create a displacement field acting on the entire system. This field is calculated by using a continuum linear Green's function,[7] which gives the displacement due to a unit force acting in a specified direction in the presence of the crack.[8,9] The resulting displacement field is thus a sum of Green's functions with origins at each of the Region-II atoms. As we

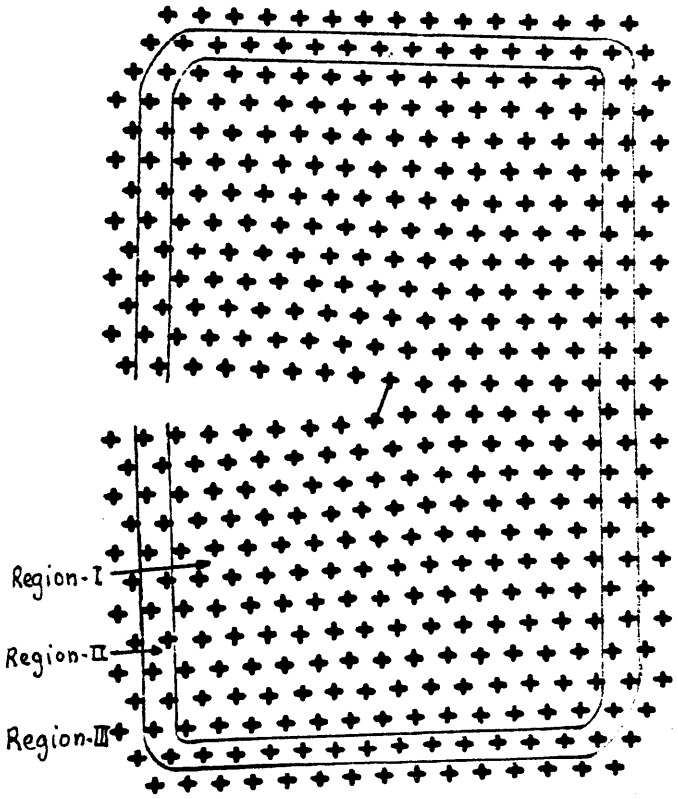

Figure 4.1 Regions for the flexible boundary method in the case of a crack tip.

will see in the next sections the Green's function diverges logarithmically at the point where the force is applied so an additional step must be used to move Region-II atoms. In the present procedure this step is a relaxation of Region-II atoms using the frictional damping method discussed above.

If the resulting forces on Region-II atoms are not small enough, the last steps are iterated until all the atoms in Regions-I and II have forces below some chosen tolerance level. A synopsis of the total procedure constituting the flexible boundary is the following:

(a) Generation of the atomic configuration of the defect according to a linear continuum solution. Division of the system into three regions.

(b) Relaxation of Region-I using CMD.

(c) Displacement of Regions-I and II according to the Green's function for the crack problem.

(d) Relaxation of Region-II atoms using CMD.

(e) Iteration of steps b, c, and d until total forces over atoms in Regions-I and II are below a prescribed magnitude.

4.1.1 Crack Tip Elastic Field

In proceeding to an analysis of the plane-crack problem it is useful to distinguish three basic modes of crack-surface displacement. Mode I corresponds to normal separation of the crack walls under the action of tensile stresses; Mode II (sliding mode) corresponds to shearing of the crack walls in a direction normal to the crack front; Mode III (tearing mode) corresponds to mutual shearing parallel to the crack front.[11] Of the three modes, the first one is the most pertinent to crack propagation in brittle solids in which we can visualize

the crack extension by progressive stretching and rupture of cohesive bonds across the crack-plane.

In our study we will concentrate on Mode I fracture where small plasticity, with possibility of formation of dislocations, can result around the crack tip. At greater distances from the crack tip the linear elasticity theory can be applied. For non-brittle solids, blunted cracks with high production of dislocations and large plastic regions around the crack tip or completely surrounding the crack can be produced.[11]

In this section we give the final solution for the linear elasticity crack tip field, stresses and displacements in the Mode I fracture, which are used in the first step of the FB technique. The standard solution to this problem involves searching for a suitable "stress function" which satisfies the "biharmonic equation" of linear elasticity theory (fourth-order differential equation including the condition of equilibrium,compatibility of strains, and Hooke's law), in accordance with appropriate boundary conditions.[10,11] The components of stress and displacements are then determined directly from the stress function.

An analytical technique has been developed by Westergaard, Muskhelishvili and others for the special case of plane-crack geometry.[12,13] The model is the "sharp crack" approximation, where it is assumed that the crack tip in the unstressed state is perfectly sharp and that the crack walls remain free of stresses.

The solutions for the field near the crack tip (i.e., at distances from the crack tip small compared to the length of the crack)

take the following analytic form for the isotropic case[10] (Fig. 4.2):

Mode I

$$\begin{Bmatrix} \sigma_{xx} \\ \sigma_{yy} \\ \sigma_{xy} \end{Bmatrix} = \frac{K_I}{(2\pi r)^{1/2}} \begin{Bmatrix} \cos\theta/2 \left[1 - \sin(\theta/2)\sin(3\theta/2)\right] \\ \cos\theta/2 \left[1 + \sin(\theta/2)\sin(3\theta/2)\right] \\ \sin\theta/2 \left[\cos(\theta/2)\cos(3\theta/2)\right] \end{Bmatrix} \qquad (4\text{-}1a)$$

$$\sigma_{xz} = \sigma_{yz} = 0 \qquad \sigma_{zz} = \nu(\sigma_{xx} + \sigma_{yy}) \text{ (plane strain)} \quad \sigma_{zz} = 0 \text{ (plane stress)}$$

$$\begin{Bmatrix} u_x \\ u_y \end{Bmatrix} = \frac{K_I}{2E}\left(\frac{r}{2\pi}\right)^{1/2} \begin{Bmatrix} (1+\nu)\left[(2K-1)(\cos\theta/2) - \cos(3\theta/2)\right] \\ (1+\nu)\left[(2K+1)\sin(\theta/2) - \sin(3\theta/2)\right] \end{Bmatrix} \qquad (4\text{-}1b)$$

$$u_z = 0 \text{ plane strain} \qquad u_z = -(\nu z/E)(\sigma_{xx} + \sigma_{yy}) \text{ plane stress}$$

where $K = (3-\nu)/(1+\nu)$ for plane stress, $K = (3-4\nu)$ for plane strain, E is the Young's modulus and ν the Poisson's ratio. The quantity K_I is called the stress-intensity factor; it is dependent on the boundary conditions of the crack system. In this case its value is:

$$K_I = \sigma_{yy_\infty}\sqrt{\pi c} \qquad (4\text{-}2)$$

σ_{yy_∞} = tensile stress, Mode I, applied at infinity

$2c$ = crack length

We can reduce these expressions to the simple form:

$$\sigma_{ij} = K_I (2\pi r)^{-1/2} f_{ij}(\theta)$$
$$u_i = (K_I/2E)(r/2\pi)^{1/2} \qquad (4\text{-}3)$$

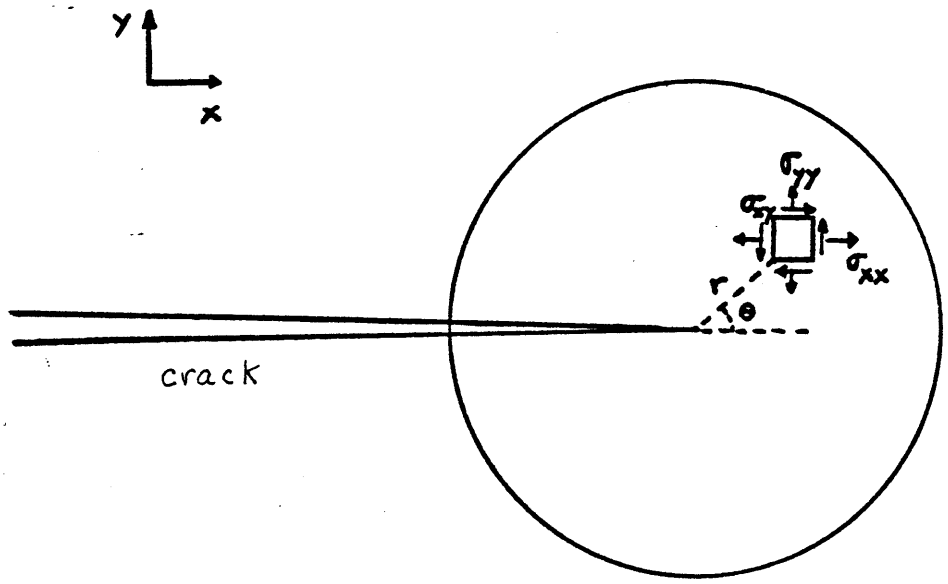

Figure 4.2 Crack tip stresses, showing components in rectangular coordinates.

The stress intensity factor depends only on the applied stress and the crack geometry; it determines the intensity of the local field. The other factors depend on the spatial coordinates about the tip, and determine the distribution of the field.

4.1.2 Atomic Relaxation

The next step of the flexible boundary technique consists in the relaxation of Region-I toward a configuration of very low forces with Region-II and Region-III atoms held fixed. As indicated before, the procedure followed here involves a frictional damping applied to the "equations of motion" after a certain period of normal simulation. The final temperature, after application of frictional damping, is reduced to approximately 3°K. Further damping to still lower temperatures does not lead to any significantly different configuration of the relaxed atomic positions.

4.1.3 Green's Function

The next step of our procedure which is different from the previous flexible boundary methods is to generate a new displacement field based on the residual forces on Region-II atoms. These forces arise from the constraint imposed by Region-III, composed of atoms displaced according to a continuum linear elasticity solution, over Region-I.

The displacement field necessary to cancel these forces is calculated by a sum of Green's functions corresponding to each force on Region-II atoms. The Green's function[7] gives the displacement field caused by a unit point force applied in a certain direction at some distance from the crack. This Green's function must include the

influence of the crack surfaces on which the boundary conditions must be satisfied (no forces can act normal to a free surface).

The resulting displacement field due to the Green's function has been calculated by Hirth et al.[8] for the case of isotropic materials. The displacement field due to the image forces which cancel the normal stresses on the two crack surfaces is:

$$
\begin{aligned}
u_1 = \frac{F_1\kappa}{4\pi(\kappa+1)\mu}\Bigg\{ & \ln \rho E - \left(\frac{\kappa+\kappa^{-1}}{2}\right)\ln \rho D + \gamma(\kappa-\kappa^{-1})\eta \\
& + \frac{P\gamma \sin\theta}{D}\left(\cos\frac{\theta-\varphi}{2} + P\cos\theta\right) - \frac{P\sin\theta}{D}\left(\sin\frac{\theta-\varphi}{2} + P\sin\theta\right) \\
& - \frac{P\gamma\sin\theta}{\kappa E}\left(\cos\frac{\theta+\varphi}{2} + P\cos\theta\right) + \frac{P\sin\theta}{\kappa E}\left(\sin\frac{\theta+\varphi}{2} + P\sin\theta\right) \\
& + \frac{\gamma\sin\varphi}{D}\left(\cos\varphi + P\cos\frac{\theta-\varphi}{2}\right) - \frac{\sin\varphi}{D}\left(\sin\varphi - P\sin\frac{\theta-\varphi}{2}\right) \\
& - \frac{\gamma\sin\varphi}{\kappa E}\left(\cos\varphi + P\cos\frac{\theta+\varphi}{2}\right) + \frac{\sin\varphi}{\kappa E}\left(\sin\varphi + P\sin\frac{\theta+\varphi}{2}\right) \\
& + \frac{P\gamma\sin\theta\sin\varphi}{\kappa D^2}\left[\sin\frac{\theta-3\varphi}{2} + 2P\sin(\theta-\varphi) + P^2\sin\frac{3\theta-\varphi}{2}\right] \\
& + \frac{P\sin\theta\sin\varphi}{\kappa D^2}\left[\cos\frac{\theta-3\varphi}{2} + 2P\cos(\theta-\varphi) + P^2\cos\frac{3\theta-\varphi}{2}\right]\Bigg\}
\end{aligned}
$$

$$
\begin{aligned}
u_2 = \frac{F_1\kappa}{4\pi(\kappa+1)\mu}\Bigg\{ & \gamma\ln \rho E - \gamma\frac{(\kappa+\kappa^{-1})}{2}\ln \rho D - (\kappa-\kappa^{-1})\eta \\
& + \frac{P\gamma\sin\theta}{D}\left(\sin\frac{\theta-\varphi}{2} + P\sin\theta\right) + \frac{P\sin\theta}{D}\left(\cos\frac{\theta-\varphi}{2} + P\cos\theta\right) \\
& - \frac{P\gamma\sin\theta}{\kappa E}\left(\sin\frac{\theta+\varphi}{2} + P\sin\theta\right) - \frac{P\sin\theta}{\kappa E}\left(\cos\frac{\theta+\varphi}{2} + P\cos\theta\right) \\
& + \frac{\gamma\sin\varphi}{D}\left(\sin\varphi - P\sin\frac{\theta-\varphi}{2}\right) + \frac{\sin\varphi}{D}\left(\cos\varphi + P\cos\frac{\theta-\varphi}{2}\right) \\
& - \frac{\gamma\sin\varphi}{\kappa E}\left(\sin\varphi + P\sin\frac{\theta+\varphi}{2}\right) - \frac{\sin\varphi}{\kappa E}\left(\cos\varphi + P\cos\frac{\theta+\varphi}{2}\right) \\
& + \frac{P\gamma\sin\theta\sin\varphi}{\kappa D^2}\left[\cos\frac{\theta-3\varphi}{2} + 2P\cos(\theta-\varphi) + P^2\cos\frac{3\theta-\varphi}{2}\right] \\
& - \frac{P\sin\theta\sin\varphi}{\kappa D^2}\left[\sin\frac{\theta-3\varphi}{2} + 2P\sin(\theta-\varphi) + P^2\sin\frac{3\theta-\varphi}{2}\right]\Bigg\}
\end{aligned}
\qquad (4\text{-}4a)
$$

where F_1 and F_2 are the point forces in the x and y directions, $\gamma = F_1/F_2$, $K = 3-4\nu$ for plane strain, μ is the shear modulus, ν, the Poisson's ration and

$$D = 1 + P^2 + 2P\cos\frac{\theta+\varphi}{2}$$

$$E = 1 + P^2 + 2P\cos\frac{\theta-\varphi}{2}$$

$$\eta = \tan^{-1}\frac{\sin(\varphi/2) - P\sin(\theta/2)}{\cos(\varphi/2) + P\cos(\theta/2)}$$

$$P = (r/\rho)^{1/2}$$

r, θ and ρ, φ are the cylindrical coordinates defining the positions of the force source and point where the displacement is evaluated.

The field of the forces themselves that gives the total field when added to the displacement field of the image forces has been derived by Hirth[9] and Eshelly.[15] The displacement field is:

$$u_1 = -\frac{F_1}{4\pi\mu}\left\{\frac{2K}{K+1}\ln\rho\left[1+P^4-2P^2\cos(\theta-\varphi)\right]^{1/2} + \frac{1}{K+1}\frac{\left[2(\sin\varphi - P^2\sin\theta)^2 - \gamma\sin 2\varphi - \gamma P^4\sin 2\theta + 2\gamma P^2\sin(\theta+\varphi)\right]}{\left[1+P^4-2P^2\cos(\theta-\varphi)\right]}\right\}$$

$$u_2 = \frac{F_1}{4\pi\mu}\left\{-\gamma\frac{2K}{K+1}\ln\rho\left[1+P^4-2P^2\cos(\theta-\varphi)\right]^{1/2} + \frac{1}{K+1}\frac{\left[-2\gamma(\cos\varphi - P^2\cos\theta)^2 + \sin 2\varphi + P^4\sin 2\theta - 2P^2\sin(\theta+\varphi)\right]}{\left[1+P^4-2P^2\cos(\theta-\varphi)\right]}\right\} \qquad (4\text{-}4b)$$

We rederived these results following the procedure indicated by Hirth.[7] An elastic and isotropic Green's function is calculated in the same way as for the evaluation of potential fields in electrostatics. In this case, there is a correspondence between the elastic displacement $\vec{u}$ and the electrostatic potential V and between the sources generating the fields, force $\vec{f}$, and the charge density ρ. One finds that the ith component of the displacement $u_{ij}(\vec{r}-\vec{r}')$ caused by a

unit point force $\delta(\vec{r}')$ applied in the jth direction at the point $\vec{r}'$ is[7]

$$u_{ij}(\vec{r}-\vec{r}') = \frac{1}{8\pi\mu}\left\{\delta_{ij}\nabla^2|\vec{r}-\vec{r}'| - \frac{\lambda+\mu}{\lambda+2\mu}\left(\frac{\partial^2|\vec{r}-\vec{r}'|}{\partial x_i \partial x_j}\right)\right\} \quad (4-5)$$

$u_{ij}(\vec{r}-\vec{r}')$ is called the Green's function for the elastic displacements of an isotropic system with *Lamé* constants λ and μ. A continuous distribution of forces $f_j(\vec{r}')$ in an elastic medium causes displacements

$$u_i(\vec{r}) = \int_V u_{ij}(\vec{r}-\vec{r}')\, f_j(\vec{r}')\, dv'$$

Equation (4-5) gives the response of an infinite body to a point force. In a finite body, boundary conditions must be satisfied. The displacements in a finite body subjected to a point force can be described as a superposition of the displacements (4-5) and displacements caused by "image" forces applied on the external surface of the body in order to satisfy boundary conditions.

In our case we have rederived Eqs. (4-4b) applying (4-5) and (4-6) to the case of two line forces $\vec{F}_x\,\delta(x')\,\delta(y')$ and $\vec{F}_y\,\delta(x')\,\delta(y')$. The forces are uniformly distributed along a line parallel to the Z axis. $\vec{F}_x$ and $\vec{F}_y$ are the forces per unit length directed in the x and y direction respectively.

The method we have applied is a powerful procedure for the solution of problems in the continuum theory of elasticity. For example, the displacement field due to point and line defects (interstitials, dislocations, etc.) can be easily determined if the response of the

body to a point force (4-4) or a line force (4-4b) is known. The interstitial solution would be given by the displacement field due to three perpendicular double forces, and an edge dislocation by the displacement field of two line forces coupled without moment.

To make an estimate of the range of validity of the continuum Green's function, a comparative study has been done between the elastic displacement provided by this function and the displacement obtained using CMD at short distances from the point force. The CMD experiment consisted of applying an external unit point force at the center of a perfect lattice and calculating the final displacement field. The external force was applied to an atom surrounded by an infinite lattice with the boundary atoms located according to the continuum Green's function (Eq. (4-4b). The final CMD displacement field gave values about 2% less than the Green's function for the first nearest neighbors while at greater distances from the source the discrepancy was much less. Therefore, the lattice Green's function can be applied at distances greater than or equal to the nearest neighbor separation. The asymmetry of the displacement field in the CMD case is due to the non-linear effects of the potential function.

Distance from the force (Interatomic spacings)	-3	-2	-1	0	1	2	3
Green's function (Å)	0.2518	0.2582	0.2692	∞	0.2692	0.2582	0.2518
CMD (Å)	0.2510	0.2563	0.2652	0.2828	0.2659	0.2569	0.2514

Table 4.1 Atomic displacements (Å) given by the Green's function of a unit point force directed in the positive x direction and CMD simulation. The displacements have been measured at several interatomic spacings from the force along the x axis. The interatomic spacing is 4.1290Å.

4.2 Computer Molecular Dynamics Determination of Elastic Constants in a Two-Dimensional Triangular Lattice

The macroscopic elastic constants of a 2-D triangular lattice have been determined by CMD. The system is composed of rare gas atoms interacting with nearest neighbors through a Lennard-Jones potential. The CMD simulation was conducted by applying different kinds of stress on the free surfaces of the system, which is composed of an 8x8 array of particles.

The elastic constants were determined in the limit of small deformations where the linear elasticity theory can be applied. A frictional damping procedure was used during the atomic relaxation. The final position of static equilibrium corresponds to a state of minimum total potential energy and its variation during the experiment must be equal to the work done by the exterior forces.

The present model is similar to the one studied by Ashurst and Hoover.[16,17] They have assumed a two-dimensional triangular crystal in which particles interact with nearest neighbors springs of elastic constant K. Their calculations showed the isotropic form of the stress-strain relations and the *damé* constants were: $\lambda = \mu = \sqrt{3}\,K/4$ (See Eq. (4-11).)

The validity of the Ashurst-Hoover analytical results was tested independently by our CMD experiments. Both cases gave the same results for $K = \left.\frac{\partial^2 V_{i,j}}{\partial r^2}\right|_{equilibrium}$, where the equilibrium position corresponds to the interatomic distance between nearest particles. Logically, for small displacements, any potential would give the same elastic constants if its curvature at the position of equilibrium $\propto \left.\frac{\partial^2 V}{\partial r^2}\right|_{equilibrium}$ is fitted to the same value.

By linear elasticity theory,[18,19] the elastic constants in a two-dimensional crystal are completely specified if the tensor T is known:

$$\sigma = \overline{\overline{T}}\,\epsilon$$

in two dimensions

$$\begin{vmatrix} \sigma_{xx} \\ \sigma_{yy} \\ \sigma_{xy} \end{vmatrix} = \begin{vmatrix} C_{11} & C_{12} & C_{13} \\ C_{21} & C_{22} & C_{23} \\ C_{31} & C_{32} & C_{33} \end{vmatrix} \cdot \begin{vmatrix} \epsilon_{xx} \\ \epsilon_{yy} \\ \epsilon_{xy} \end{vmatrix} \qquad (4-7)$$

where[18] $C_{ij} = C_{ji}$ $\qquad \sigma_{xy} = \sigma_{yx}$

and $C_{31} = C_{32} = C_{13} = C_{23} = 0$

The calculations of the four constants, C_{11}, C_{12}, C_{22} and C_{33}, were performed in four separate CMD simulations.

(A) Simulation 1 - Calculation of C_{22}.

In this calculation we began with the equation

$$\sigma_{yy} = C_{21}\epsilon_{xx} + C_{22}\epsilon_{yy}$$

We made $\epsilon_{xx} = 0$ by ensuring no atomic displacements in the x direction, then

$$\sigma_{yy} = C_{22}\epsilon_{yy}$$

where $\sigma_{yy} = f/d$, $\epsilon_{yy} = L-L_o/L_o$, f is the exterior force acting on each atom, d, the nearest neighbor interatomic spacing and L, L_o the final and original length of the system respectively. C_{22} is determined from the slope of the curve σ_{yy} versus ϵ_{yy} at the origin. Strains were also calculated by measuring the relative deformations within

the system. In this way the boundary effects were avoided.

(B) Simulation 2 - Determination of C_{21}.

$$\sigma_{yy} = C_{21}\,\epsilon_{xx} + C_{22}\,\epsilon_{yy}$$

Now, we let contractions of the system in the x-direction while applying a stress σ_{yy}. The two strains ϵ_{xx} and ϵ_{yy} were measured and the value of C_{22} was known from Simulation 1.

(C) The same procedure was employed to calculate C_{11}, but now applying a stress in the x-direction. The symmetry of the $\bar{T}$ tensor was checked by determining C_{12}. As expected from the isotropic form of $\bar{T}$ (Eq. (4-11)), the values found for C_{11} and C_{12} resulted equal to C_{22} and C_{21} respectively.

(D) Finally, to determine C_{33} ($\sigma_{xy} = C_{33}\,\epsilon_{xy}$) a shear stress, tangent force to the free surface, was applied on each surface atom, whereby definition, $\epsilon_{xy} = \tan\theta \simeq \theta$. The resulting elastic coefficients for our 2-D lattice are

$$\begin{aligned} C_{11} &= C_{22} = 1256.16 \ \text{dynes/cm} \\ C_{12} &= C_{21} = 418.72 \ \text{dynes/cm} \\ C_{33} &= 837.44 \ \text{dynes/cm} \end{aligned} \qquad (4-10)$$

If we express Eq. (4-7) in the form:

$$\begin{vmatrix} \sigma_{xx} \\ \sigma_{yy} \\ \sigma_{xy} \end{vmatrix} = \begin{vmatrix} \lambda+2\mu & \lambda & 0 \\ \lambda & \lambda+2\mu & 0 \\ 0 & 0 & 2\mu \end{vmatrix} \begin{vmatrix} \epsilon_{xx} \\ \epsilon_{yy} \\ \epsilon_{xy} \end{vmatrix} \qquad (4-11)$$

the value of the *Lamé* constants λ and μ can be determined using (4-10)

$$\lambda = \mu = 418.72 \text{ dynes/cm}$$

We can see that these values, determined by CMD, coincide with the analytical calculations of Ashurst and Hoover, assigning to the constant K the value $\left.\frac{\partial^2 V_{L\text{-}J}}{\partial r^2}\right|_{\text{equilibrium}} = 967 \text{ dynes/cm}$

The determination of the elastic constants E, Young's modulus, and ν, Poisson's ratio, was carried out by inverting the tensor $\bar{T}$.

$$\epsilon = \bar{T}^{-1}\sigma$$

$$\begin{vmatrix} \epsilon_{xx} \\ \epsilon_{yy} \\ \epsilon_{xy} \end{vmatrix} = \begin{vmatrix} S_{11} & S_{12} & S_{13} \\ S_{21} & S_{22} & S_{23} \\ S_{31} & S_{32} & S_{33} \end{vmatrix} \begin{vmatrix} \sigma_{xx} \\ \sigma_{yy} \\ \sigma_{xy} \end{vmatrix} \qquad (4\text{-}12)$$

where, by definition

$$E = \frac{\sigma_{yy}}{\epsilon_{yy}} = S_{22}^{-1} = 1116.59 \frac{\text{dynes}}{\text{cm}} \quad (\sigma_{xx} = \sigma_{xy} = 0) \qquad (4\text{-}13a)$$

and

$$\nu = -\frac{\epsilon_{xx}}{\epsilon_{yy}} = \frac{-S_{12}}{S_{22}} = \frac{1}{3} \quad (\sigma_{xx} = \sigma_{xy} = 0) \qquad (4\text{-}13b)$$

In the following CMD experiments we have used the elastic constants derived in this section. When it was necessary to use elastic continuum solutions in three dimensions, for example in step-1 of FB, where the initial configuration of the defect was generated, and in step-3 where Green's function was applied, we have used the equivalence between our 2-D case and the 3-D plane strain with the same *Lamé* constants.[16]

Surface energy is another physical constant of great importance in mechanics of fracture. In our case we need it to determine the theoretical Griffith's critical stress. The surface energy is taken as the work required to completely separate the crystal along some given plane starting from the undeformed perfect configuration.

When the atomic forces are specified by a potential function and there is a finite cut-off distance, the surface energy is given by the difference of energy on the potential curve between the static position of equilibrium and the cut-off distance which would correspond to the energy to break a bond times the number of bonds per unit area along the plane of crack propagation.

We have determined by using this procedure the surface energy of the Lennard-Jones system and three Morse potentials. The values are listed in Table 5.1 of the next chapter.

4.3 Application of Flexible Boundary to a Two-Dimensional Crack Tip

The procedure described in Section 4.1 has been applied to a two-dimensional triangular lattice whose atoms interact through a Lennard-Jones potential, Fig. 4.3.

To demonstrate the efficiency of the flexible boundary technique as applied to small systems, several tests were carried out with different numbers of particles and two different stresses. Figure 4.4a shows the variation of the crack tip bond length with the size of the system for a stress intensity factor close to the Griffith's critical value, which has been determined using the elastic constants and surface energy of the system (Section 4.2)

$$\left(\sigma \cdot \sqrt{\pi c}\right)_c = \sqrt{2E\gamma} = 3.21 \cdot 10^{-2} \ \text{dynes} \cdot \text{cm}^{-1/2}$$

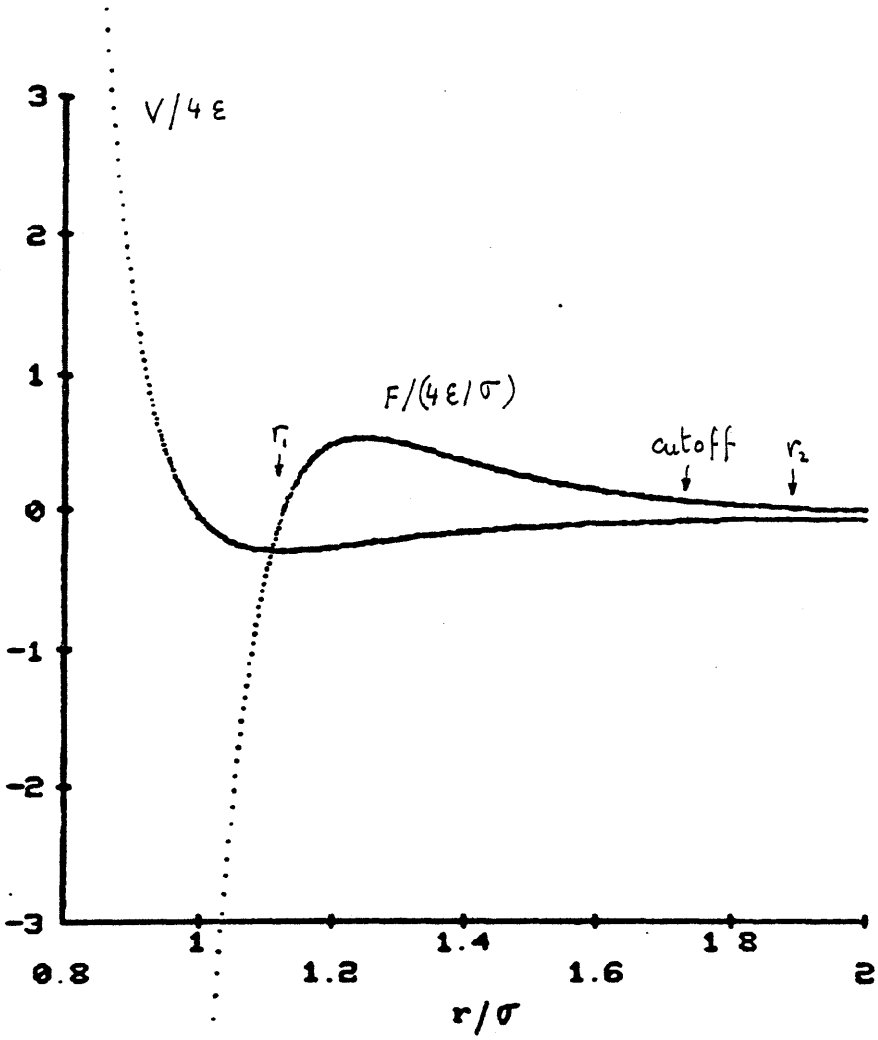

Figure 4.3 Potential function and force of a Lennard-Jones rare gas. The first nearest neighbor (r_1) is located at the minimum of the potential $2^{1/6}\sigma$. The cut-off range is 1.7σ and further interaction was neglected.

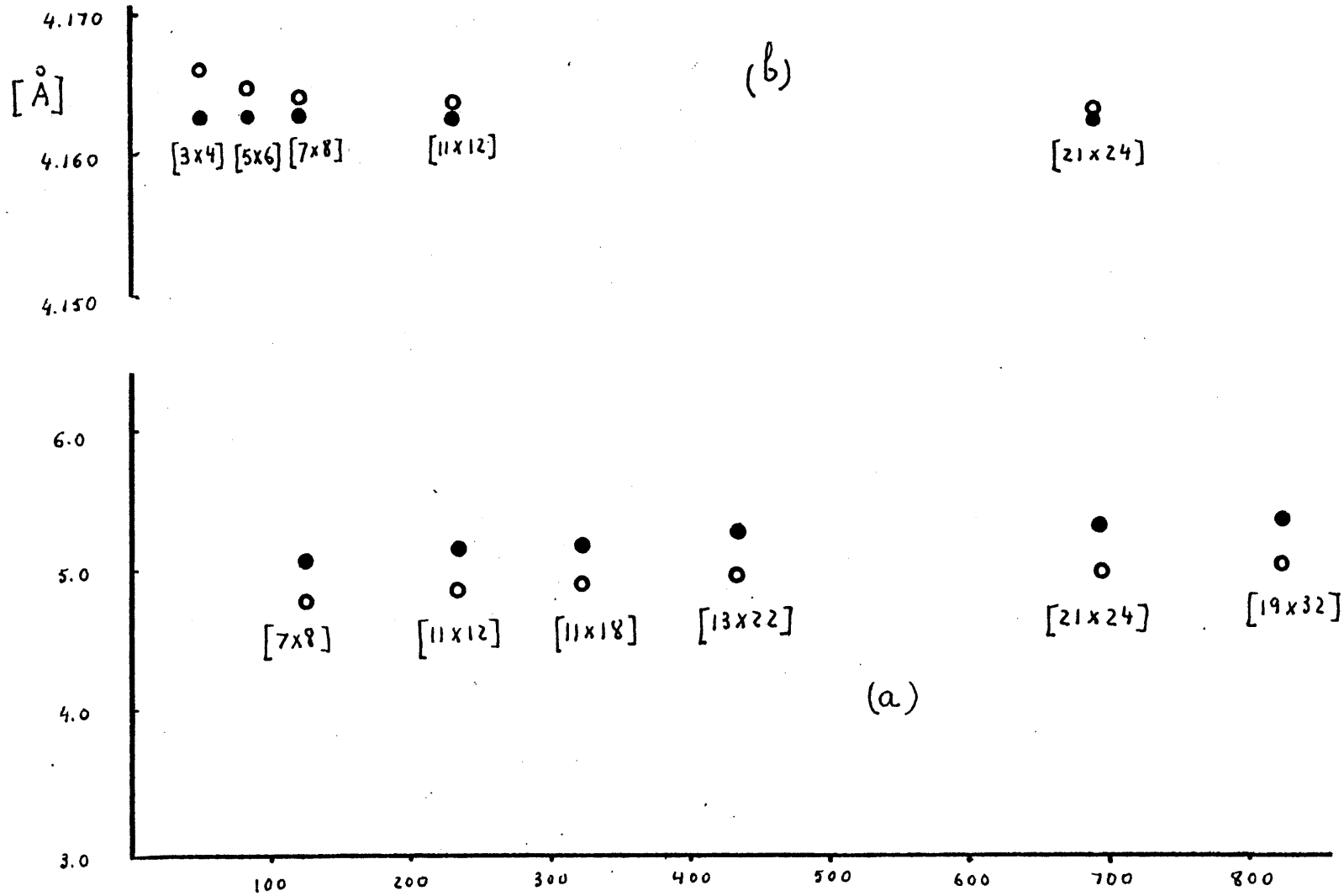

Figure 4.4 a - b Variation of crack tip bond length with system size. [axb] denotes the number of particles along x and y direction in Region-I. Results for fixed boundary condition (0), flexible boundary condition (●). (a) $\sigma\sqrt{\pi c}=3.17\cdot10^{-2}$ dynes $cm^{-1/2}$. (b) $\sigma\sqrt{\pi c}=3.17\cdot10^{-3}$ dynes $cm^{-1/2}$.

The high efficiency of the procedure is shown in Fig. 4.4b where a small stress intensity factor was applied to ensure that the linear elasticity theory is valid at any point of the system. The configuration of equilibrium using FB could be sufficiently accurately determined with a small system composed of only 84 particles whereas considerably larger systems were required to obtain the same crack tip bond length using fixed boundary condition.

At high stresses, where a non-linear region exists around the crack tip, the flexible boundary procedure is not any more efficient, as Fig. 4.4a shows the results given by FB vary with the size of the system about as much as the results obtained with fixed boundary. The reason for this behavior is probably that the elastic continuum Green's function, which is responsible for the final displacement of the boundaries, has been derived assuming the system is entirely composed of a linear elastic material and does not consider the non-linear properties of the region surrounding the crack tip. This effect is clearly more important at high stresses and when the system size is no longer large compared to the size of the non-linear region. In this case it will be necessary to work with larger systems in order to obtain the correct crack tip configuration.

Table 4.2 shows the variations with system size of the maximum force acting on atoms in Region-I and Region-II. Also given are the crack tip bond lengths obtained with fixed and flexible boundaries.

If the forces acting on Region-II atoms are zero after the relaxation of Region-I, we can assume that the continuum linear elasticity theory is valid in this region and that the boundaries do not impose

$\sigma\sqrt{\pi c} = 3.17 \cdot 10^{-3}$ dynes $cm^{-1/2}$

number of particles	shape of region-I	maximum force acting on a R-II atom (initial configuration)	maximum force acting on a R-II atom after 1st relaxation	crack tip bond length (σ) fixed boundary	flexible boundary
82	5x6	$0.29 \cdot 10^{-8}$ dynes/atom	$0.19 \cdot 10^{-7}$ dynes/atom	1.1320	1.1315
126	7x8	$0.13 \cdot 10^{-8}$ "	$0.12 \cdot 10^{-7}$ "	1.1319	1.1315
234	11x12	$0.42 \cdot 10^{-9}$ "	$0.72 \cdot 10^{-8}$ "	1.1318	1.1315
694	21x24	$0.28 \cdot 10^{-9}$ "	$0.36 \cdot 10^{-8}$ "	1.1317	1.1315

$\sigma\sqrt{\pi c} = 3.17 \cdot 10^{-2}$ dynes $cm^{-1/2}$

126	7x8	$0.89 \cdot 10^{-7}$ dynes/atom	$0.31 \cdot 10^{-6}$ dynes/atom	1.31	1.38
234	11x12	$0.64 \cdot 10^{-7}$ "	$0.23 \cdot 10^{-6}$ "	1.32	1.40
324	11x18	$0.69 \cdot 10^{-7}$ "	$0.19 \cdot 10^{-6}$ "	1.34	1.42
436	13x22	$0.60 \cdot 10^{-7}$ "	$0.13 \cdot 10^{-6}$ "	1.35	1.44
694	21x24	$0.36 \cdot 10^{-7}$ "	$0.14 \cdot 10^{-6}$ "	1.36	1.45
822	19x32	$0.40 \cdot 10^{-7}$ "	$0.10 \cdot 10^{-6}$ "	1.37	1.45

Table 4.2 Tests of convergence using flexible boundary.

any constraint on the crack tip. Unfortunately, the magnitude of these forces decreases very slowly by increasing the number of particles (fourth column of Table 4-2) being necessary to use very large systems to assume that the continuum solution at the boundaries is valid. Flexible boundaries provide a procedure to cancel these forces for small systems and as we have seen its efficiency only decreases in the presence of large non-linear regions around the crack tip.

Figures 4-5 to 4-16 show the strain fields and rotations around the crack tip at different stages of the computations: (a) initial step or continuum elasticity solution, (b) after relaxation of Region-I, fixed boundary and (c) after the application of FB. The principal strains and rotations have been calculated using the procedure given in the next chapter.[20]

The difference between fixed and flexible boundaries is shown in Figs. 4.5a, b and c, where a stress intensity factor $\sigma\sqrt{\pi c}$ equal to $1.13(\sigma\sqrt{\pi c})_c^{theo}$ was applied. The critical value $(\sigma\sqrt{\pi c})_c^{theo}$ corresponds to the theoretical value derived by Griffith and was calculated from the elastic constants and surface energy of the system.

Figure 4.5b shows the crack tip configuration after the relaxation of Region-I, fixed boundary. The crack tip bond length has not reached the maximal permissible length, which corresponds to the cut-off of the potential, so one may conclude on this basis that the critical value of the stress intensity factor is greater than $1.13(\sigma\sqrt{\pi c})_c^{theo}$. However, as shown in Fig. 4.5c, which corresponds to a configuration obtained with FB, the crack tip bond has already reached the maximum bond length at a stress intensity factor of

$1.13(\sigma\sqrt{\pi c})_c^{theo}$, and the crack is propagating by breaking bonds. Therefore, the critical stress intensity factor is actually less than $1.13(\sigma\sqrt{\pi c})_c^{theo}$.

Figures 4.6 and 4.7 show the principal strain fields and rotations around the crack tip for the different boundaries. The linear elasticity solution, Eq. (4-1a), yields a state of biaxial tensile strain in front of the crack tip and higher values of shear deformation at 60° and 120° from the positive x axis (see Fig. 4.6a). The non-linear effects given by CMD simulations are shown in Figs. 4.6b and 4.6c, which correspond to the amplifications of these fields in the immediate vicinity of the crack tip. The brittleness of the material has not changed substantially the distribution of the strain around the crack tip and the only remarkable characteristics are the higher values of the strains when the FB procedure was applied.

The absence of dislocation in this material which would indicate a brittle behavior can be explained by applying the Kelly, Tyson and Cottrell criterion (KTC) discussed in Chapter Three. This criterion for brittle behavior is

$$\left(\frac{\sigma_{SHEAR}}{\sigma_{COHESIVE}}\right)_{ideal} > \left(\frac{\sigma_{SHEAR}}{\sigma_{COHESIVE}}\right)_{max}$$

where the second term depends on the maximum values attained at the crack tip. Its value according to linear elasticity theory is 0.5 for mode - 1 fracture.

The ideal shear and cohesive stresses were determined by two separate simulations, where a shear and a biaxial tensile stress were

applied to a perfect lattice (Figs. 4.10 and 4.11). We will show in the next chapter that the ideal shear stress determined in this way is an overestimate. As proposed by Orowan[21] we have taken for the ideal shear stress the value determined in a simulation where the atomic sliding in the x direction is accompanied by a small displacement in the positive y-direction (Fig. 3.11, dashed line). The relation between the ideal shear and cohesive stress is 0.83, implying that the system should show brittle behavior.

Finally, it has been found that the stress intensity factor necessary to break the crack tip bonds and propagate the crack is higher than predicted by Griffith's theory.

$$\text{CMD} \quad (\sigma\sqrt{\pi c})_c = 3.35 \cdot 10^{-2} \text{ dynes cm}^{-1/2} \quad (2\text{-D})$$

$$\text{Griffith's Theory} \quad (\sigma\sqrt{\pi c})_c = 3.21 \cdot 10^{-2} \text{ dynes} \cdot \text{cm}^{-1/2} \quad (2\text{-D})$$

The CMD critical stress intensity factor was determined by applying successively higher values to $\sigma\sqrt{\pi c}$ until crack propagation was obtained.

The critical value depends on the atomic model used in the simulation. In our case we have assumed no interaction between atoms situated on different crack surfaces. If interaction is possible when the distance between a pair of atoms is less than the cut-off range of the potential function the stress intensity factor can be higher than the value obtained above. Similar results were found by Gehlen et al.[22] in the case of α-iron, the critical stress intensity factor being about three times the Griffith value. These results are not

surprising for several reasons. First, Griffith's criterion is considered a necessary condition but not sufficient for crack propagation. Secondly, Griffith's equations are based upon macroscopic linear elasticity continuum properties. They do not consider energy balance on a local, atomic scale or generation of dislocation at the crack tip, although the last possibility was not observed in this material. Further discussion of these results and some of the recently developed atomic models which could explain this behavior is given in the last chapter.

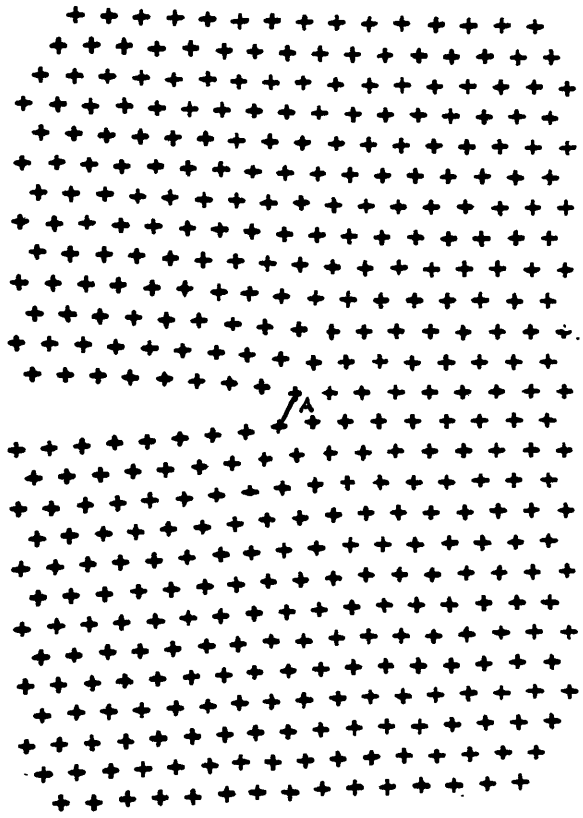

Figure 4.5a Initial atomic configuration based on linear elasticity theory of a two-dimensional crack embedded in an infinite medium. Sytem consists of 436 particles arranged in a triangular lattice. The crack tip bond is shown by the line segment A, its length is less than the cut-off of the potential function.
$\sigma\sqrt{\pi c}=1.13(\sigma\sqrt{\pi c})^{\text{theoretical}}_{c}$.

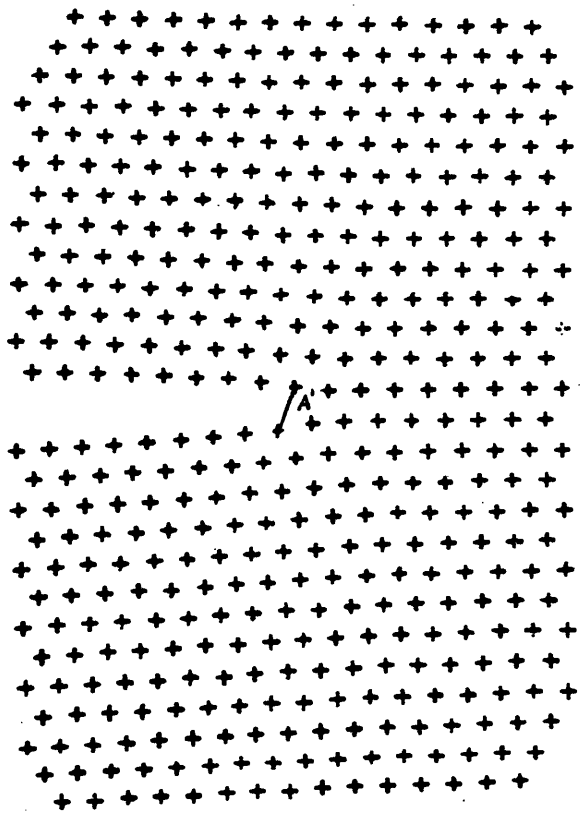

Figure 4.5b Same system as Fig. 4.5a after the relaxation of Region-I (fixed boundary). The crack tip bond is A'. Its length is now 10% greater than A (Fig. 4.5a) but still less than the cut-off range of the potential. However, relaxation of the forces acting on the particles at the boundaries, by using FB, reveals that the critical stress intensity factor has been exceeded (see next figure).

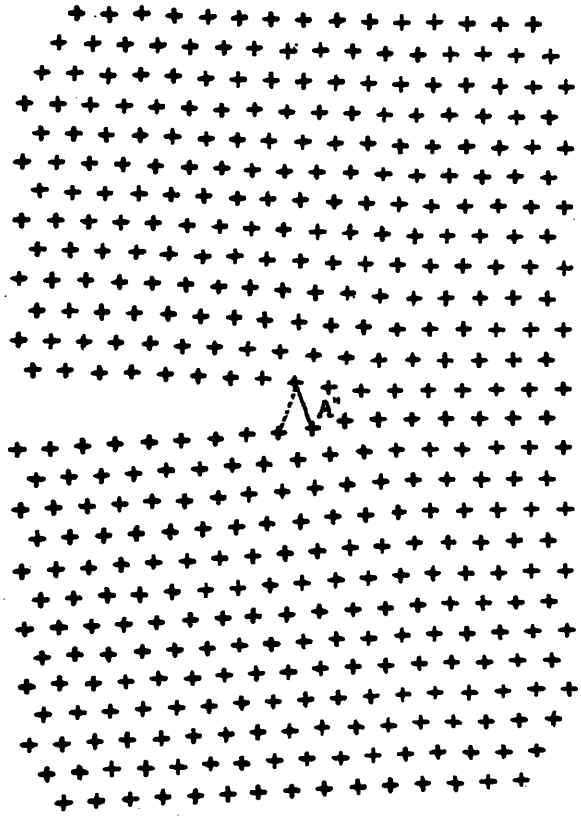

Figure 4.5c Atomic configuration using flexible boundary. The crack starts to propagate by breaking bonds because the critical stress intensity factor was exceeded. The crack tip bond is now A". Previous crack tip bonds have been broken (dashed lines).

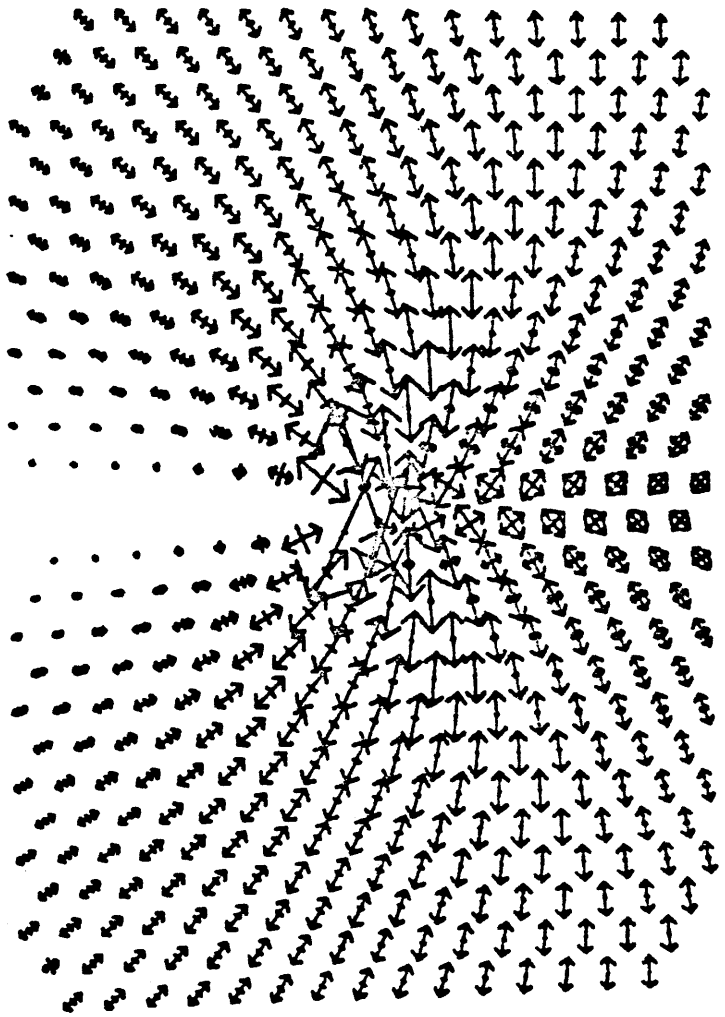

Figure 4.6a Principal strains at the initial configuration (linear elasticity theory) ↕ dilatation strain, | compressive strain.

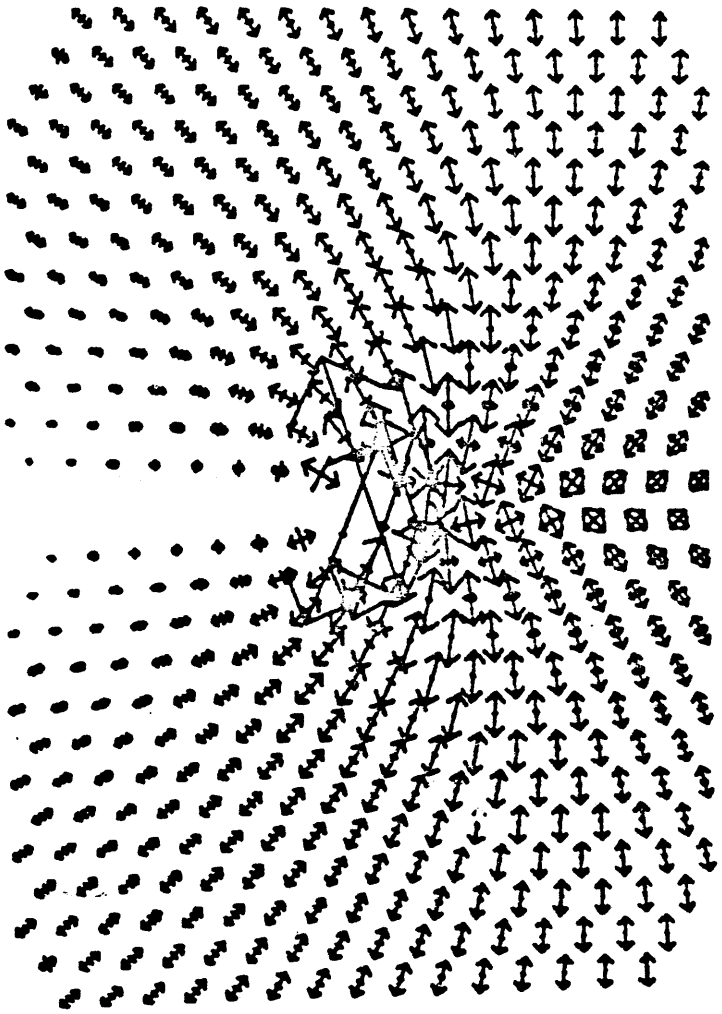

Figure 4.6b Principal strains after the first relaxation (fixed boundary) ↕ dilatation strain, | compressive strain.

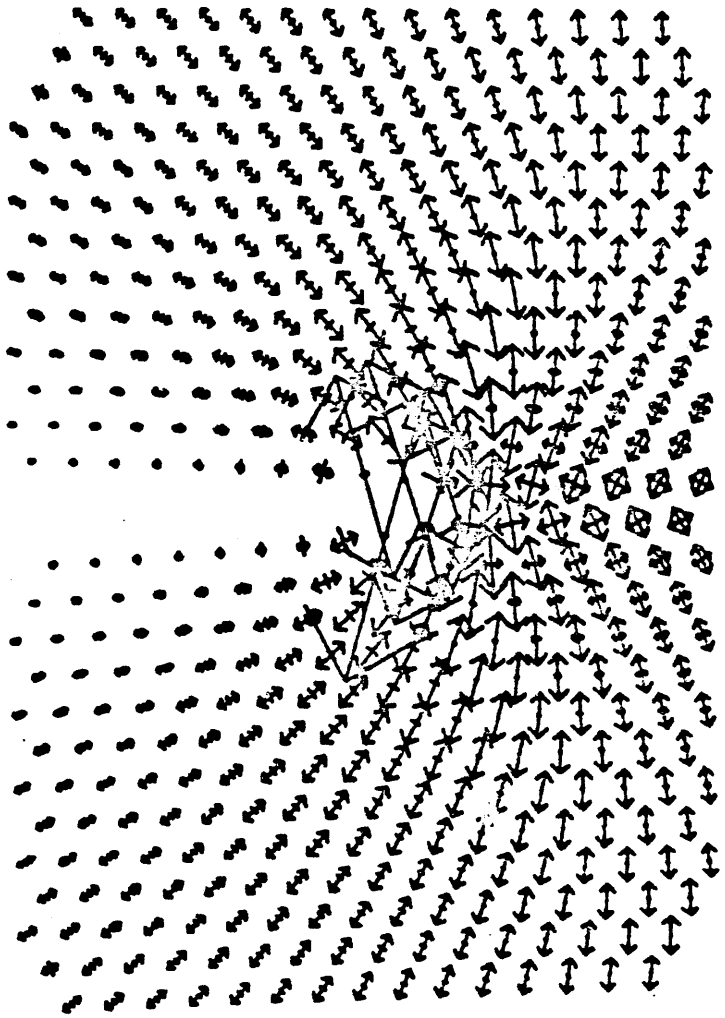

Figure 4.6c Principal strains in the final relaxed configuration (flexible boundary). ↕ dilatation strain, | compressive strain.

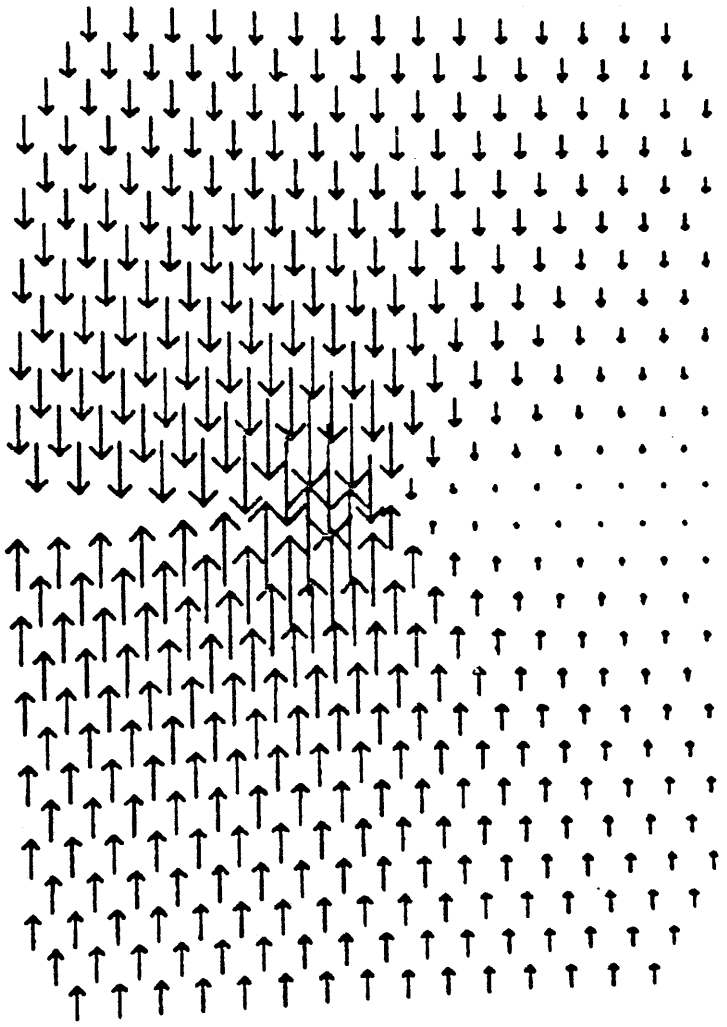

Figure 4.7a Rotations at the initial configuration (linear elasticity theory) ↑ indicates magnitude and direction of the rotation.

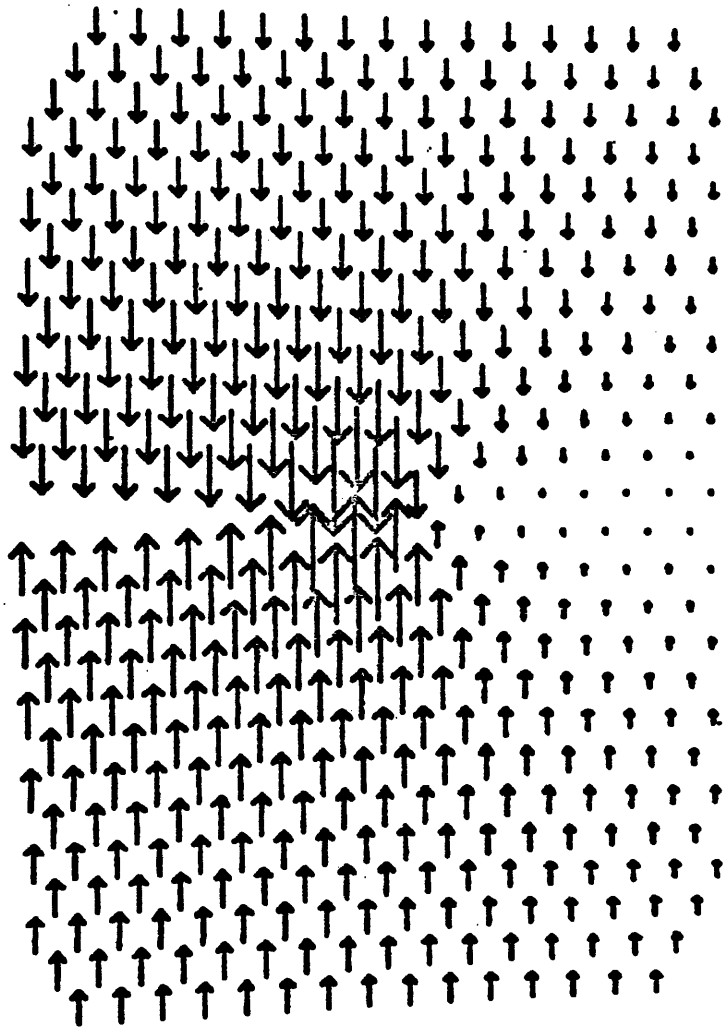

Figure 4.7b Rotations after the first relaxation (fixed boundary) ↑ indicates magnitude and direction of the rotation.

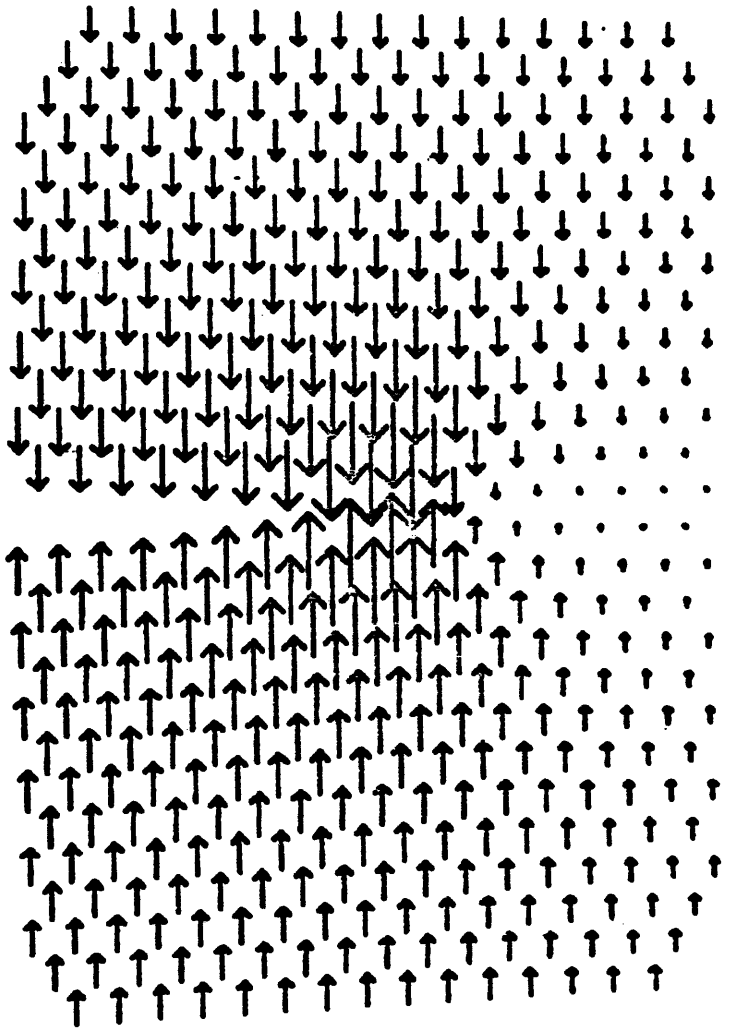

Figure 4.7c Rotations after applying flexible boundary. ↑ indicates magnitude and direction of the rotation.

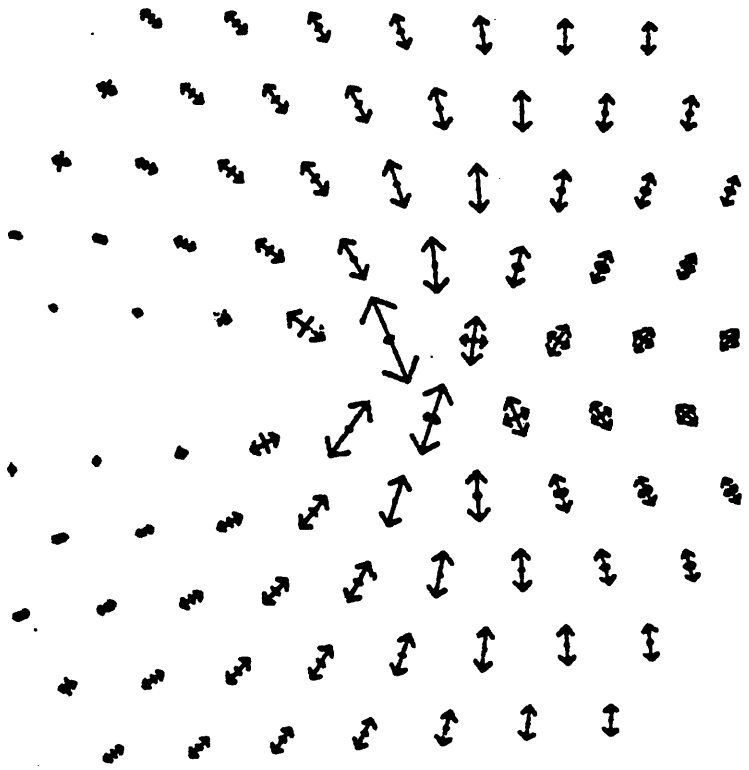

Figure 4.8a Principal strains at the initial configuration (linear elasticity theory) ↕ dilatation strain, | compressive strain.

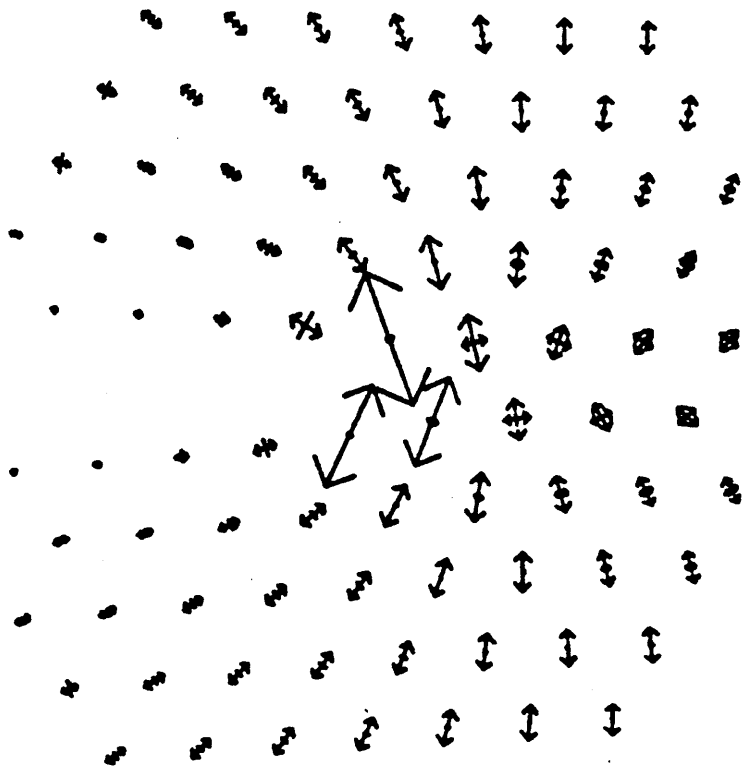

Figure 4.8b Principal strains after the initial relaxation (fixed boundary) ↕ dilatation strain, | compressive strain.

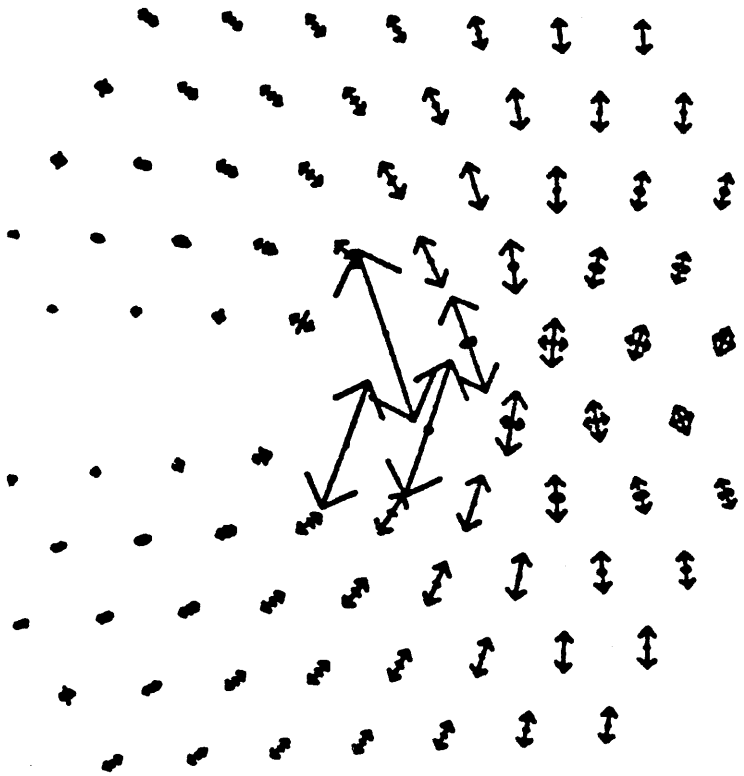

Figure 4.8c Principal strains (flexible boundary) ↕ dilatation strain | compressive strain.

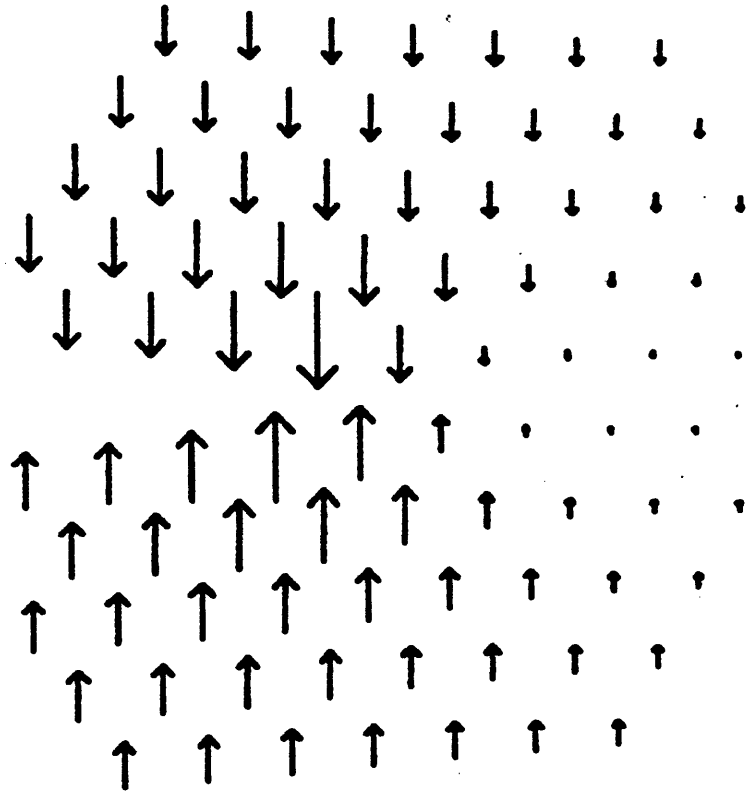

Figure 4.9a Rotation field at the initial configuration (linear elasticity theory). ↑ indicates magnitude and direction of rotation.

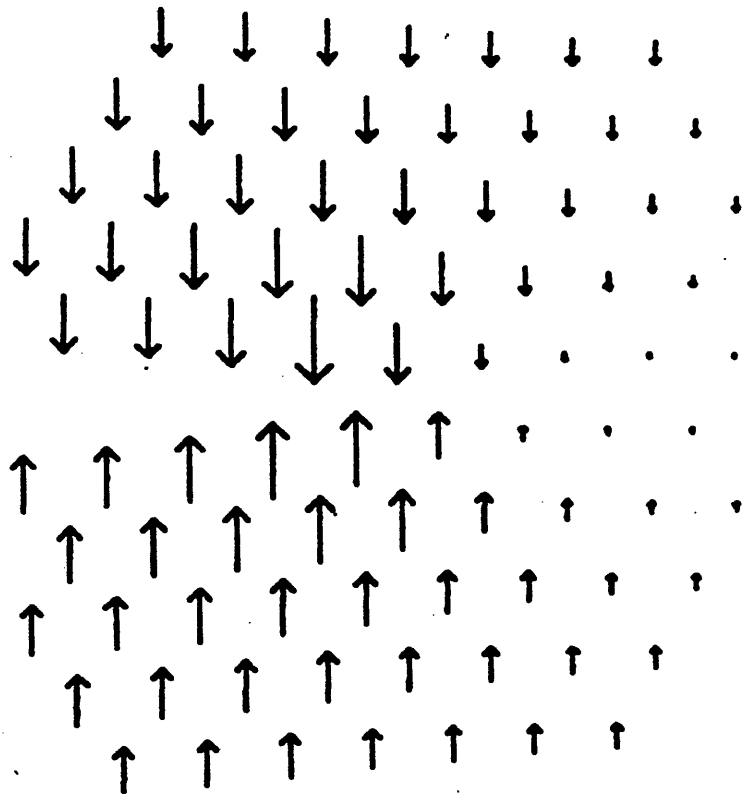

Figure 4.9b Rotation field. Fixed boundary. ↑ indicates magnitude and direction of rotation.

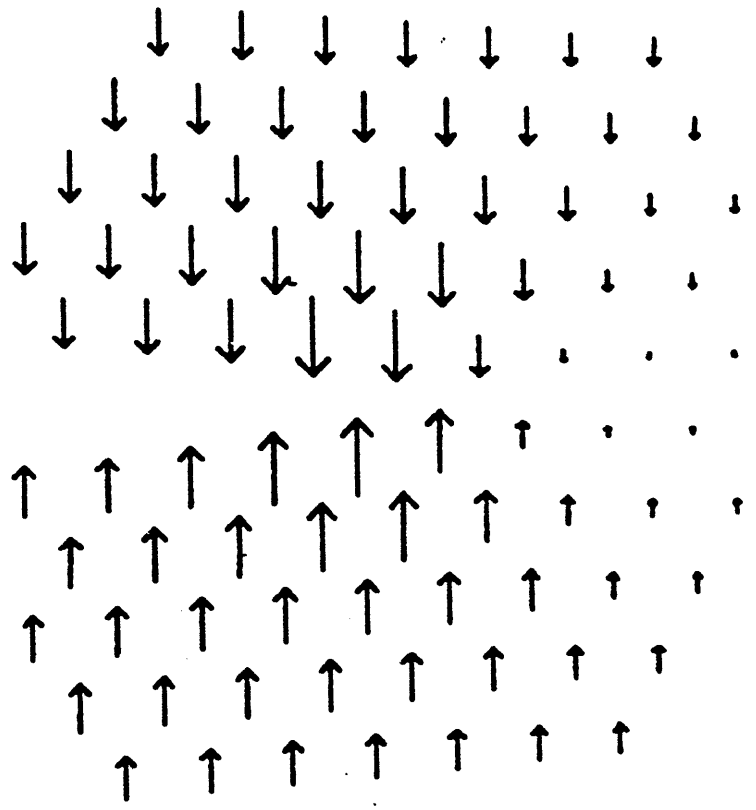

Figure 4.9c Rotation field. Flexible boundary. ↑ indicates magnitude and direction of rotation.

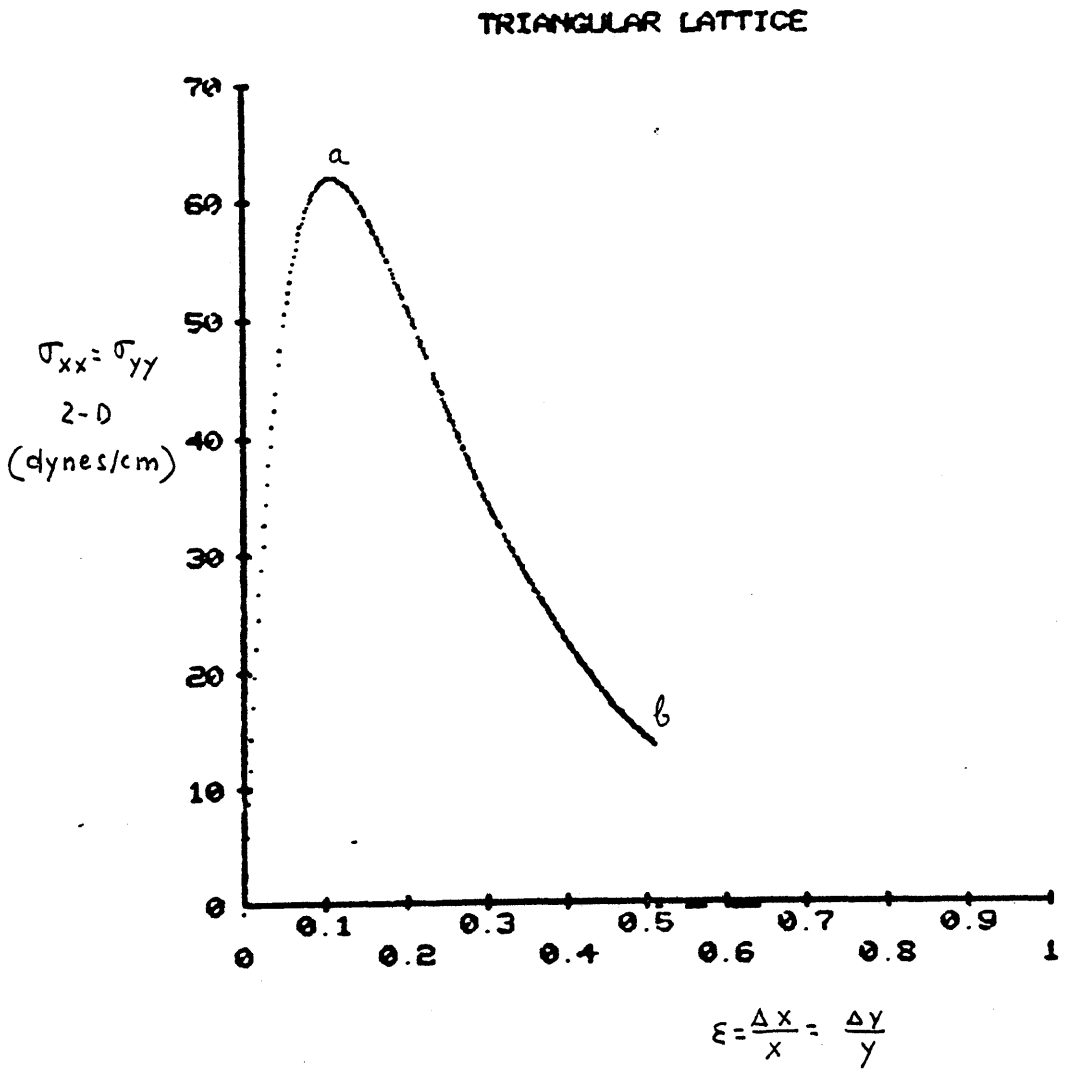

Figure 4.10 Biaxial stress versus strain in the case of a uniform expansion of a perfect lattice whose atoms interact through a Lennard-Jones potential (Kr). Point a on the curve corresponds to the ideal cohesive stress, point b is the rupture point, where all the atomic bonds reach the cut-off distance of the potential function.

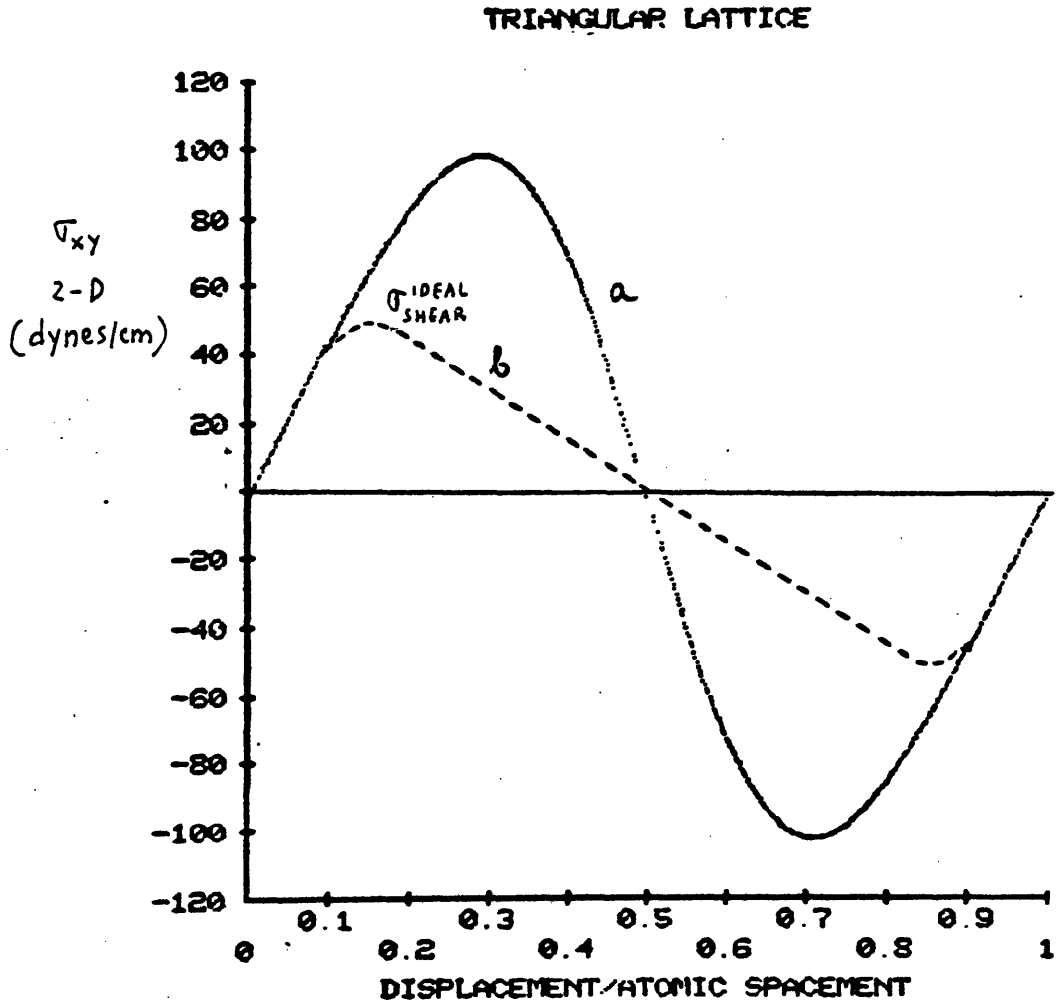

Figure 4.11 Shear stress versus displacement for the shearing of two rows of atoms which interact through a Lennard-Jones potential (Kr). Curve a was obtained with displacements along the x direction. Curve b permitted simultaneous relaxation along the y direction.

Chapter Five

Computer Molecular Dynamics Studies of Plastic Deformation around a Crack Tip

5.1 Introduction

Two continuum treatements to predict brittle or ductile behavior from known material properties have been studied using CMD. In addition to these two tests, the strain fields due to several atomistic processes of plastic relaxation around the crack tip have been determined.

The first section of this chapter summarizes the Rice and Thomson (RT)[1] and Kelly, Tyson and Cottrell (KTC)[2] criteria for predicting brittle or ductile behavior. Section two describes the atomistic model used in the simulation. Several properties of the material, elastic constants and ideal stresses, were determined in additional tests by applying CMD to a block of perfect lattice under different states of stress. The continuum criteria to predict brittle or ductile behavior, KTC and RT, were studied and compared with atomistic preductions given by CMD. Finally the rotations and strain field due to plastic deformation around the crack tip were studied and analyzed numerically.

5.2 Ductile and Brittle Behavior

Two criteria have appeared recently to predict brittle or ductile behavior in a known material under certain states of stress. Kelly, Tyson and Cottrell proposed that brittle fracture would be observed if $(\sigma_s/\sigma_c)_{ideal} > (\sigma_s/\sigma_c)_{max}$, where the subscripts "ideal" and "max" refer respectively to the ideal properties of a perfect lattice and to the maximum values attained at a crack tip. $(\sigma_s/\sigma_c)_{max}$ is calculated using linear elasticity theory (for mode-1 fracture it is ~ 0.5) and $(\sigma_s/\sigma_c)_{ideal}$ is a property of the material. Rice and Thomson[1]

on the other hand, assumed that a necessary criterion for brittle fracture is stability against the emission of dislocations from the crack tip and have derived an analytical expression using linear elasticity and the Peierls model of a dislocation core. They used two different treatments to predict the type of fracture. The first one is based on a three-dimensional model which calculates the energy to activate a dislocation loop. The second one uses a two-dimensional model with the dislocation emitted from the crack tip lying parallel to the crack front. In both cases, three forces are supposed to be acting on the dislocation near the crack tip: (a) the force due to the stress field surrounding the crack, (b) the surface tension force caused by creating more surface at the blunted crack, and (c) the image force of the dislocation in the free surface of the crack. The first force repels the dislocation, and the other two attract it toward the crack tip, generating a position of unstable equilibrium where the resultant force is zero. Both treatments, nevertheless, produced similar quantitative results[1] and we have studied the treatment based on the two-dimensional model because it is more closely related to our simulation setup.

Figure 5.1 shows the geometry of the dislocation and the crack tip. The dislocation has a Burgers vector b_e perpendicular to the dislocation line (edge dislocation); it is emitted at an angle of 60° from the positive x axis (direction of maximum shear stress in mode-1 fracture). Under this condition the force acting on the dislocation due to the stress field produced by the crack tip in mode-1 fracture is:[3]

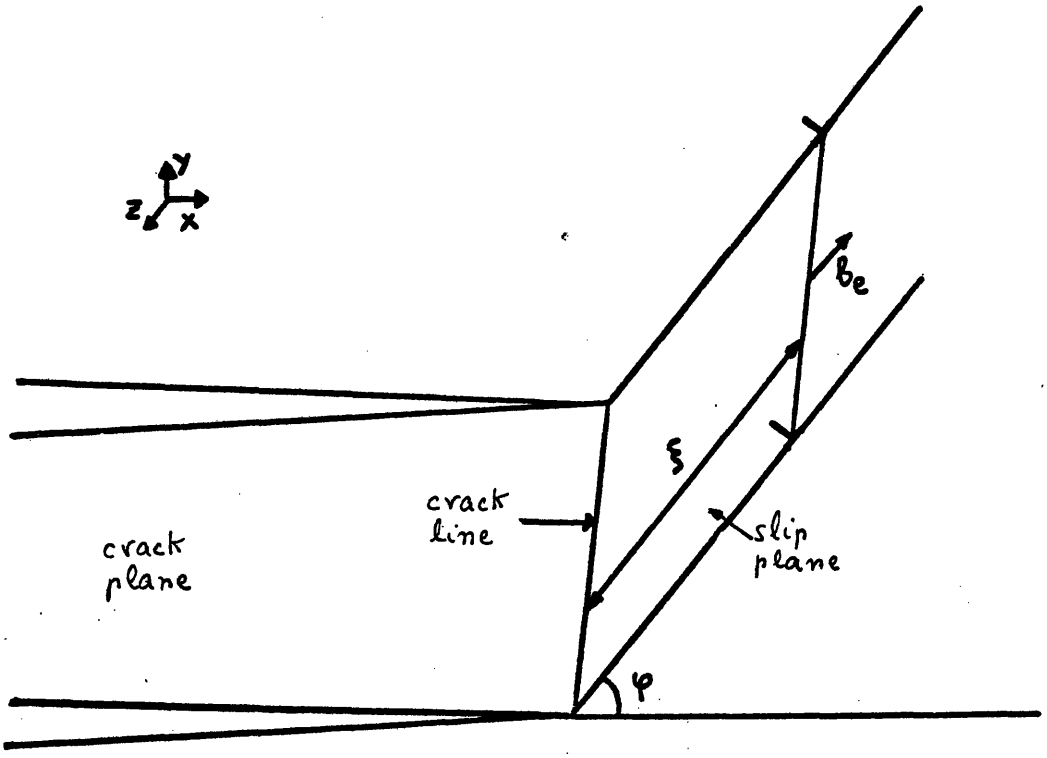

Figure 5.1 Dislocation and crack configuration. The Burgers vector b_e, perpendicular to the dislocation line, corresponds to an edge dislocation emitted by the crack tip. Rice-Thomson criterion assumes that the crack tip will be blunted by emission of dislocations (plastic behavior) when the core of the dislocation ξ_o is greater than a critical distance, ξ_c. This critical distance corresponds to a position of unstable equilibrium. For $\xi < \xi_c$ the dislocation is attracted by the crack tip and for $\xi > \xi_c$ it is repelled.

$$f_\sigma = \tau_{r\varphi}\, b_e = \frac{\sigma_{ext}\sqrt{\pi c}}{(8\pi r)^{1/2}} \sin\phi \cos(\phi/2)\, b_e = \sigma\sqrt{\pi c}\left(\frac{b}{8\pi\xi}\right)^{1/2} \frac{1}{\beta} \qquad (5-1)$$

where $\xi = r/b$, $\phi = 60°$, $1/\beta = \sin\phi\cos(\phi/2) = 3/4$, σ_{ext} and c are the exterior stress and half crack length respectively.

The attractive image force is[3]

$$f_i = \frac{-E\, b_e}{8\pi(1-\nu^2)\,\xi} \qquad (5-2)$$

where E is the Young's modulus and ν the Poisson's ratio.

The third force is produced by the surface tension when the crack is blunted (increment of free surface) and is given by

$$f_s = \frac{-2\gamma\alpha\sin\phi}{\pi(\xi^2+\alpha^2)} \qquad (5-3)$$

γ is the surface energy, $\alpha = e^{3/2}\xi_0/2$, $\xi_0 = 1/e^{3/2}(1-\nu)$

The radius of the dislocation core, ξ_0, has been determined using the Peierls model.[3]

The attractive forces, f_i and f_s, proportional to ξ^{-1} and ξ^{-2} respectively, are greater than f_σ when ξ is small, and the opposite occurs when ξ is large. Hence, if the dislocation is able to surmount the position of unstable equilibrium, ξ_c, it will be driven away until it reaches some obstacle or it cannot overcome the resistance of the lattice.

The critical distance, ξ_c, at which the dislocation reaches an unstable equilibrium is, from Eqs. (5-1), (5-2) and (5-3)

$$f_{total} = \sigma\sqrt{\pi c}\left(\frac{b}{8\pi\xi_c}\right)^{1/2}\frac{3}{4} - \frac{\mu b}{4\pi\xi_c(1-\nu)} - \frac{\sqrt{3}\gamma}{\pi}\frac{\alpha}{(\xi_c^2+\alpha^2)} = 0 \quad (5\text{-}4)$$

after replacing E by $2\mu(1+\nu)$ and making $\phi = 60°$.

At this point, the Rice-Thomson criterion assumes that if the position of equilibrium ξ_c, obtained from Eq. (5-4), is less than the dislocation core, ξ_o, spontaneous generation is possible and the crack suffers ductile fracture.

Rice and Thomson have determined the dislocation core ξ_o and the critical distance ξ_c for a wide range of materials, and based on these results they found that a sharp cleavage crack is stable in a wide range of crystal types. In general, face-centered cubic materials are able to emit dislocations. Ionic and covalent crystals are stable against dislocation emission, and the body-centered cubic crystals are intermediate between brittle and ductile materials.

5.3 Computer Molecular Dynamics Studies of Ductile versus Brittle Behavior

The simulation system we have studied is composed of 436 particles forming a triangular lattice and interacting through a Morse potential (Fig. 5.2)

$$V(r) = D\left\{\exp\left(-2\alpha(r-r_o)\right) - 2\exp\left(-\alpha(r-r_o)\right)\right\} \quad (5\text{-}5)$$

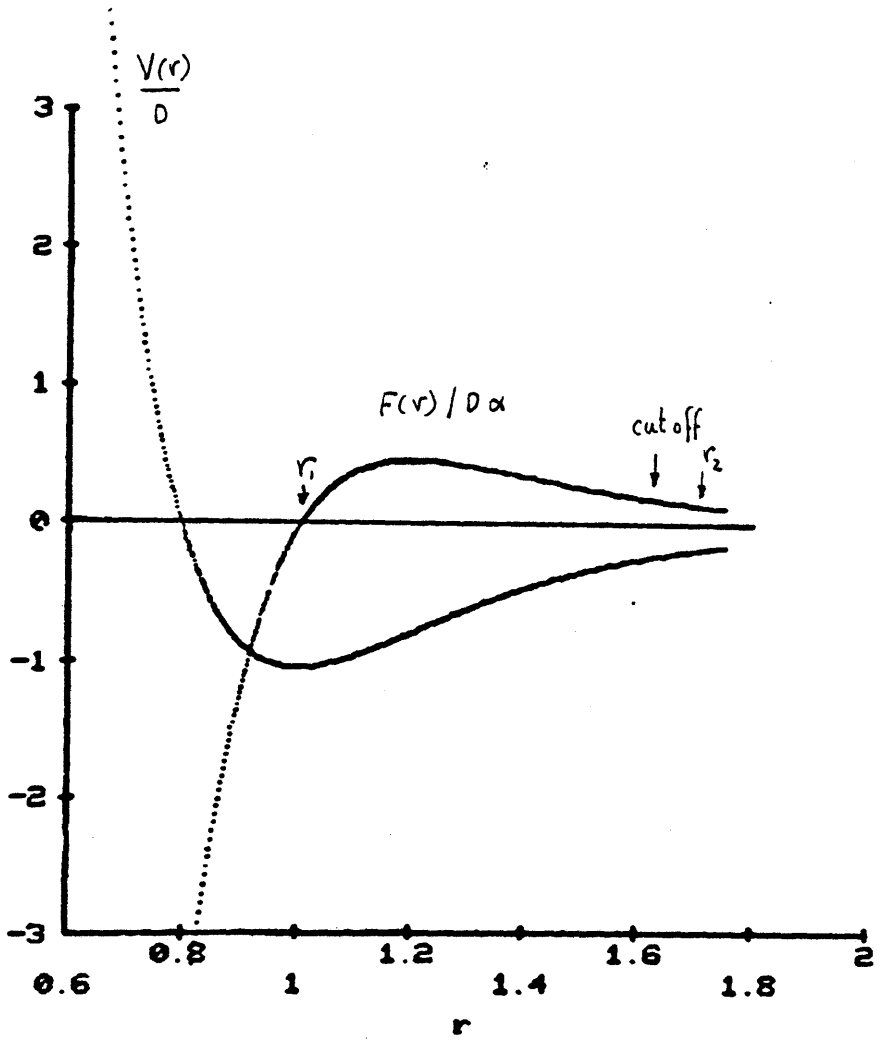

Figure 5.2 Potential function and force for Cu atoms interacting through a Morse potential $V(r) = D\left[\exp(-2\alpha(r-r_0)) - 2\exp(-\alpha(r-r_0))\right]$ with $D = 0.5892$ eV, $\alpha = 1.3543$ Å^{-1}, $r_0 = 2.5475$ Å. The first nearest neighbor is located at the minimum of the potential (r_1). The cut-off range is $1.6\, r_0$ and further interaction was neglected.

The parameters D, α and r_o were determined by Cotterill[4] and Girifalco[5] using experimental values for the energy of vaporization, the compressibility and the lattice constant of f.c.c. materials.

Fixed boundary was used in all the simulations. Under these conditions, particles on the boundaries are displaced according to a continuum elasticity solution and remain fixed during the rest of the computation (see Chapter Four).

The computer simulations were carried out with a Morse potential corresponding to Cu[4] and two other potentials of the Morse type with the parameter α modified (see Table 5-1 at the end of this chapter). The purpose of choosing different α values was to study the influence of this parameter on the emission of dislocation from the crack tip. As we will see at the end of the chapter, this parameter seems to affect also the interaction of the crack tip with the boundary, the interaction being smaller for smaller α.

In addition to the CMD experiments to determine the elastic constants of the system (Chapter 4), two different experiments were done to find the ideal cohesive stress σ_{ic} and the ideal shear stress σ_{is}. The ideal cohesive stress, σ_{ic}, can be determined by applying a homogeneous expansion to a perfect lattice until the equally extended bonds reach the maximum permissible length given by the cut-off of the potential. The maximum stress reached during the experiment corresponds to the ideal cohesive stress σ_{ic} (Fig. 5.3). The ideal shear stress, σ_{is}, can be determined following the classical experiment of Frenkel[6] which consists of the shearing of two rows of atoms in a homogeneously strained crystal (Fig. 5.4). As noted by Orowan[7] the

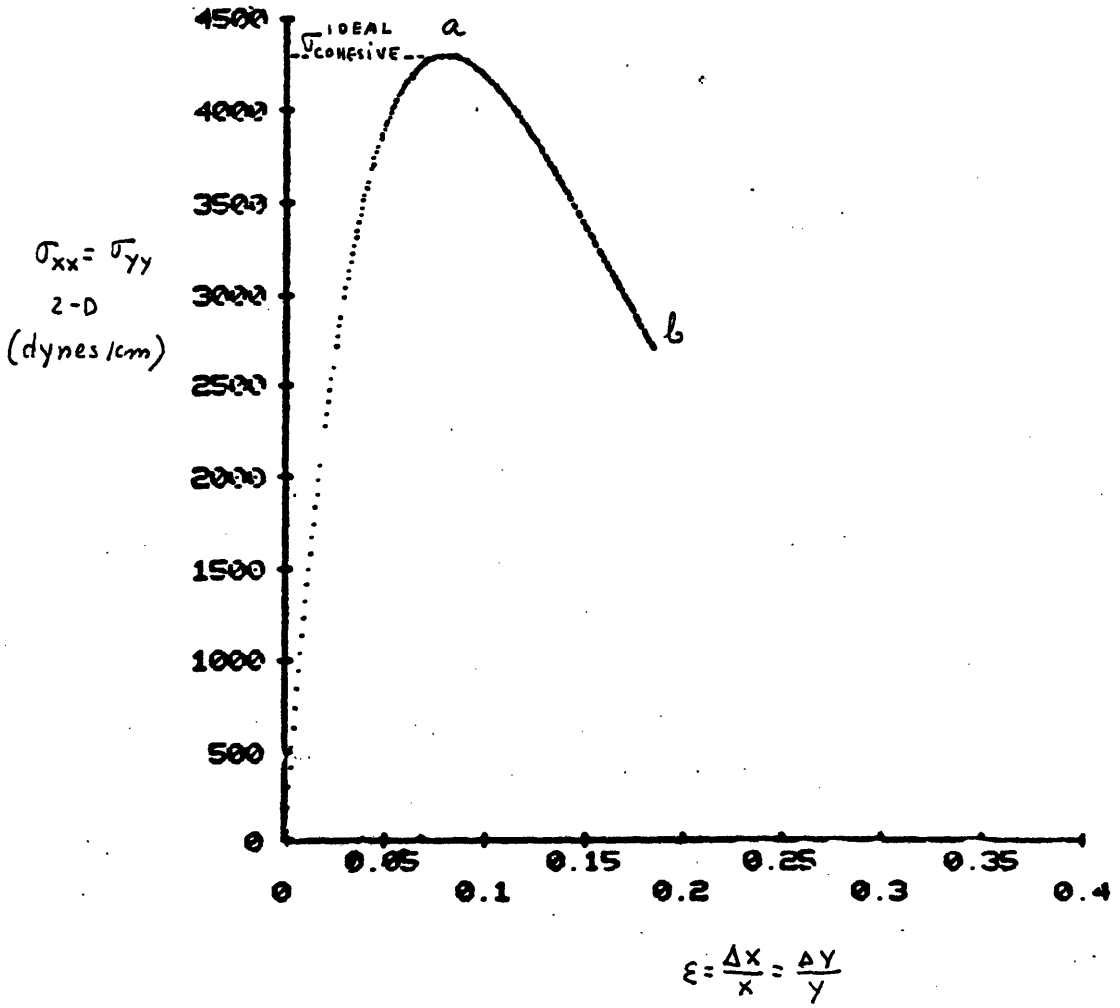

Figure 5.3 Biaxial stress versus strain for a uniform expansion of a perfect lattice whose atoms interact through a Morse potential (Cu). Point a on the curve corresponds to the ideal cohesive stress, σ_{ic}. Point b is the rupture point, where all the bonds reach the cut-off distance of the potential function.

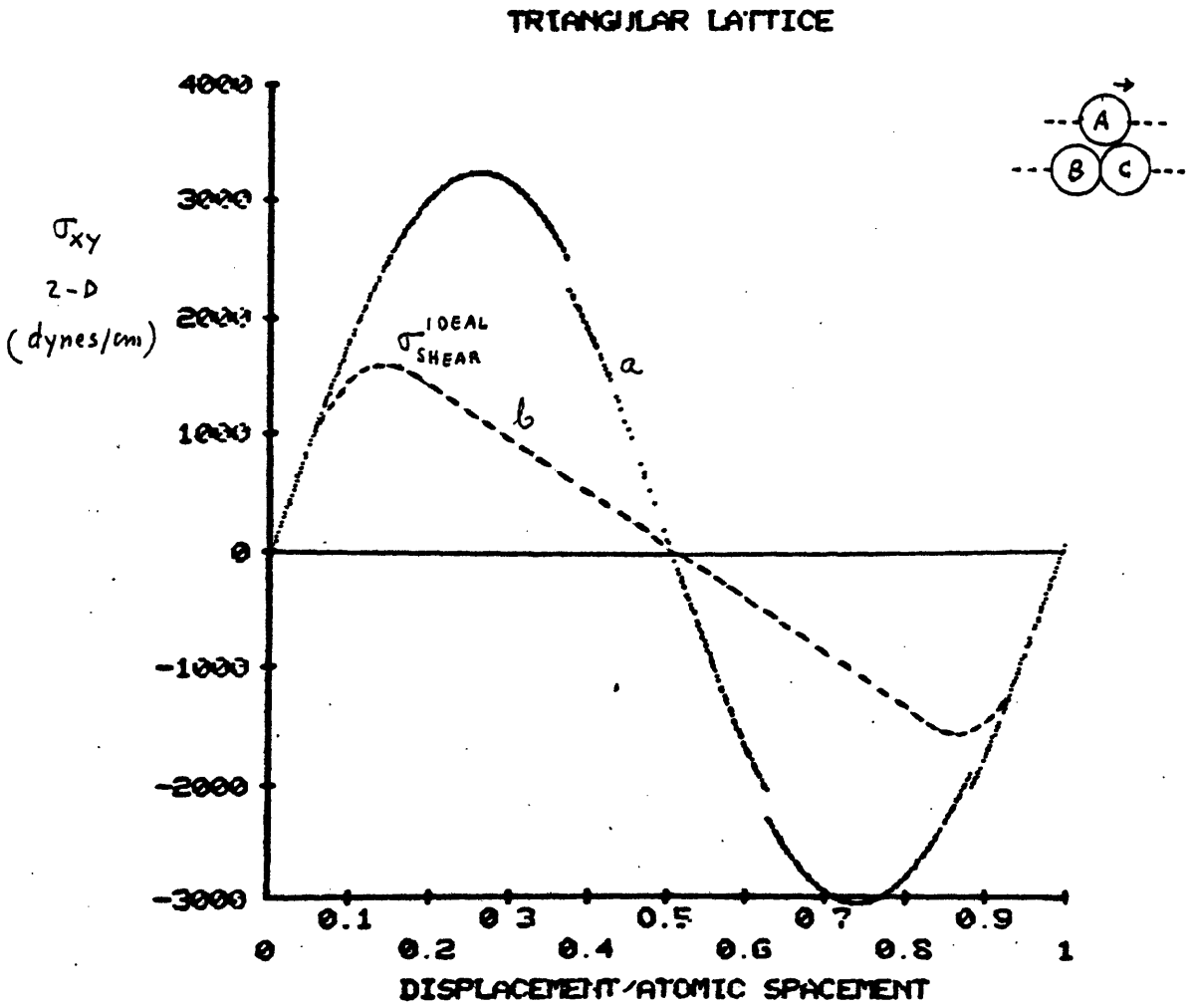

Figure 5.4 Shear stress versus displacement for the shearing of two rows of atoms which interact through a Morse potential (Cu). Curve a was obtained with displacements along the x direction. Curve b permitted simultaneous relaxation along the y direction.

ideal shear stress can be reduced (curve b) if atom A slides over atom C instead of suffering a straight displacement (curve a). This is due to the steeply repulsive part of interatomic potentials generated by the overlapping of closed shells.

The Burgers vector corresponding to a certain sheared region was determined by the equation[3]

$$b = \oint_c \frac{\partial \vec{u}}{\partial \ell} d\ell \qquad (5-6)$$

where the derivative was approximated using the differences between the displacements of two nearest neighbors.

The strain fields and rotations around the crack tip were determined using the following equation[8] (Fig. 5.5):

$$\varepsilon_{xx} = \frac{\partial u}{\partial x} = \frac{u_B - u_o}{\Delta x} \qquad \varepsilon_{yy} = \frac{\partial v}{\partial y} = \frac{v_B - v_o}{\Delta y}$$

$$\gamma_{xy} = \frac{\partial u}{\partial y} + \frac{\partial v}{\partial x} = \frac{u_B - u_o}{\Delta y} + \frac{v_B - v_o}{\Delta x} \qquad (5-7)$$

$$\omega_{xy} = \frac{\partial u}{\partial y} - \frac{\partial v}{\partial x} = \frac{u_B - u_o}{\Delta y} - \frac{v_B - v_o}{\Delta x}$$

As shown in Fig. 5.5, the relative displacements u and v were interpolated for points A and B on the intersection of lines between centers of the nearest neighbors particles and the positive x and y directions. Using these relative displacements and the initial separations Δx and Δy, local shear strains, ε_{xy}, dilatations ε_{xx}, ε_{yy} and rotations ω_{xy} were determined. With the strains, ε_{xx}, ε_{yy} and ε_{xy}, the two principal strains were calculated. These results,

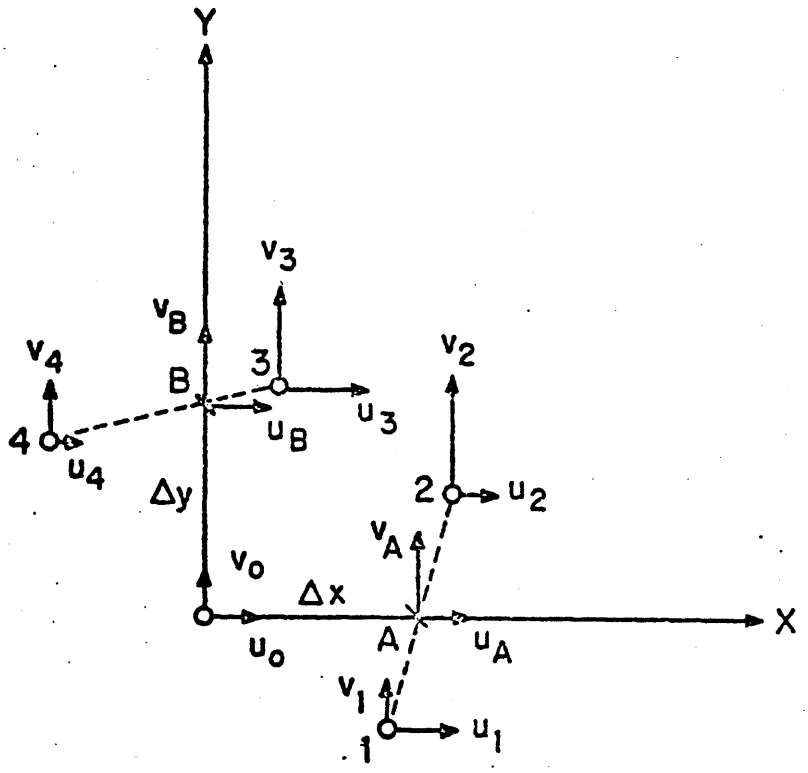

Fig. 5.5 Interpolation scheme of relative displacements of bubbles used in computing local shears and dilatations observed in sheared bubble rafts. (8)

jointly with the rotations, ω_{xy}, are shown in Figs. 5.6 to 5.11 for different configurations (before and after relaxation) and three potential functions, Fig. 5.13.

Figures 5.6a and 5.6b show the initial and final configurations in the case of a Morse potential with α equal to 0.25, M-3 potential. KTC criterion predicts ductile behavior and RT criterion brittle behavior (Table 5.2). Better estimates using RT criterion can be made by assigning ξ_o, the dislocation core, more realistic values determined by CMD.[3]

Figure 5.6b shows the Burgers vector corresponding to the sheared region enclosed in the Burgers circuit of Fig. 5.12. The Burgers circuit was taken along a region of perfect material and finished at point b to add up the effects of the small Burgers vectors corresponding to shear along the planes between points a and b. The total Burgers vector includes also the effects of the crack opening when the linear elasticity theory is applied to generate the initial configuration.

The sheared region, when a large stress intensity factor is applied (Fig. 5.6b), extends until it interacts with the fixed boundary. Figures 5.9a and 5.9b show the initial and final configuration for the same material, M-3, and a lower stress intensity factor. In this case the sheared region does not interact with the boundaries.

Figure 5.6b suggests the possibility of a phase transition from a triangular to a cubic system by rotation of the lattice. To study this kind of deformation the strain field and rotations were determined using the Eq. (5-7) (Fig. 5.7a-b and Fig. 5.8a-b). The same

studies were done with a different Morse potential, M-2, and smaller shear deformations were observed (Fig. 5.10a-b). The different behavior in the case of M-2 potential seems to be due to the steeper slope of the potential function (α=0.4). In this case, the interaction between particles has changed from "soft particles" (α=0.25) to "hard particles" (α=0.4) and slip along certain planes is now hindered by the rigid boundary (i.e., dd' Fig. 5.10b).

By increasing the parameter α to 1.3, M-1 potential, which corresponds to Cu atoms, the interaction with the boundary is even greater (see Fig. 5.11) and presumably one has to use much larger systems in order to observe the same type of sheared deformation.

The advantage of using a soft potential, M-3, despite the unrealistic value of α, is that the weak interaction with the boundary may enable one to observe, through scaling, the behavior of a more realistic potential such as M-1 in a larger system.

A graphic analogy of this case is shown in the bubble-raft model[4] where the dislocation width changes from a few interatomic spacings for soft bubbles (1.9 mm diameter) to approximately 40 interatomic spacings for hard bubbles (0.3 mm diameter). This explains again the difficulty to accommodate the dislocations emitted by the crack tip in a few interatomic spacings for the case of hard potentials.

KTC criterion predicts ductile behavior for M-2 and M-3 potentials $\left((\sigma_{ys}/\sigma_{yc})_{M-2} \simeq (\sigma_{ys}/\sigma_{yc})_{M-3} \simeq 0.06 \right)$. However, we have seen that for the M-2 potential the interaction with the fixed boundary starts to affect seriously the slip along some planes. In the case of the M-1 potential, σ_{ys}/σ_{yc} is 0.38, too close to 0.5 to make a

clear-cut prediction. The CMD simulation has shown crack propagation by breaking bonds along the crack front but the results are not completely free from boundary dependent effects by the reasons given above.

RT criterion seems not to be successful in predicting the correct behavior for potentials M-2 and M-3, where KTC criterion and CMD both predict ductile behavior. As noted by Rice and Thomson the application of linear continuum elasticity in the region close to the crack tip is an approximation and the core of the dislocation, ξ_o, has been estimated according to the Peiersls model.

A comparative study of the prediction of these two criteria has been made by Tyson[9] by compiling the results obtained with CMD. This study also shows that KTC criterion is more successful than the RT approximation.

Finally, the Lennard-Jones system studied in Chapter Four clearly behaves as a brittle material, Figs. 4.5a to 4.5c. This behavior is consistent with the high values found for σ_{ci}/σ_{cc} and ξ_c.

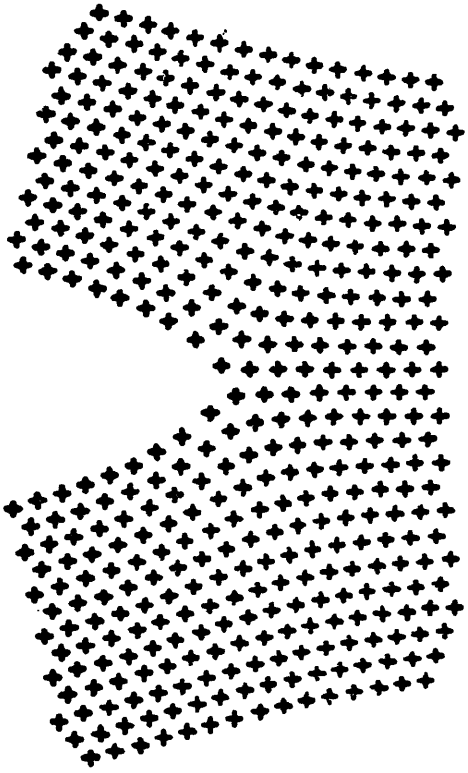

Figure 5.6a Initial atomic configuration based on linear elasticity theory of a two-dimensional crack embedded in an infinite medium. System consists of 436 particles arranged in a triangular lattice, interacting through a Morse potential (M-3).

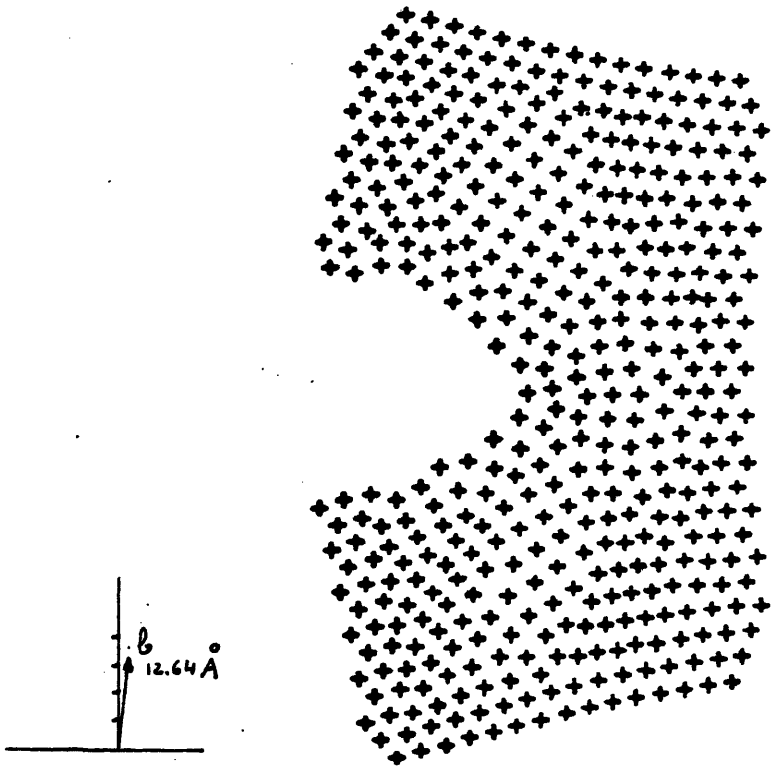

Figure 5.6b Same as Fig. 5.6a after the relaxation of the atomic region (fixed boundary). Potential M-3.

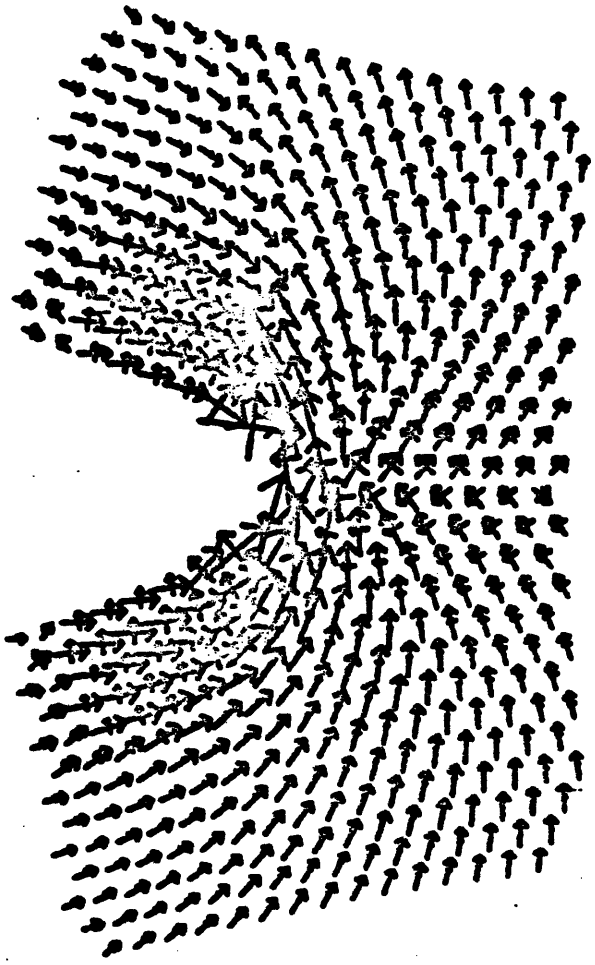

Figure 5.7a Principal strains at the initial configuration (linear elasticity theory) ↑ dilatation strain, | compressive strain.

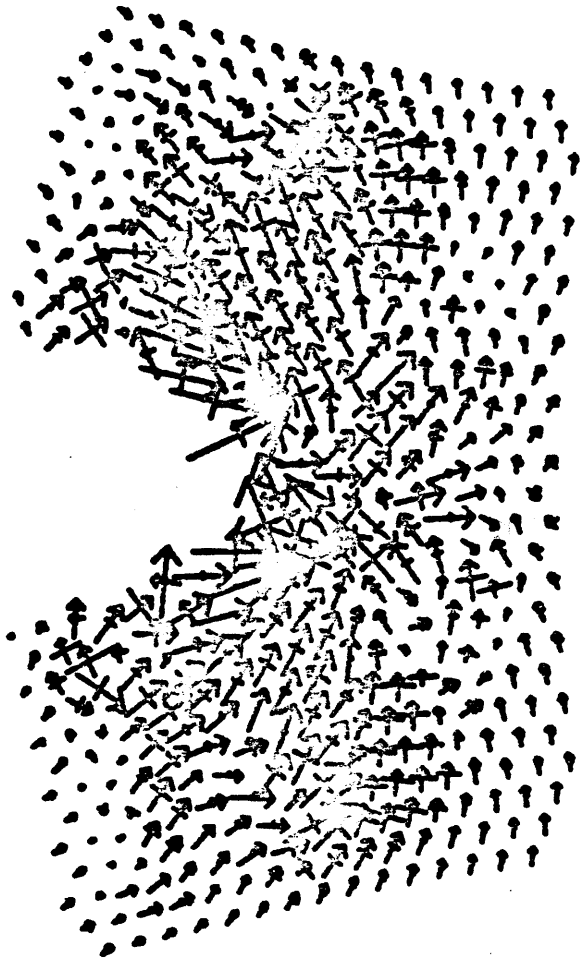

Figure 5.7b Principal strains in the final relaxed configuration (fixed boundary) ↑ dilatation strain, | compressive strain.

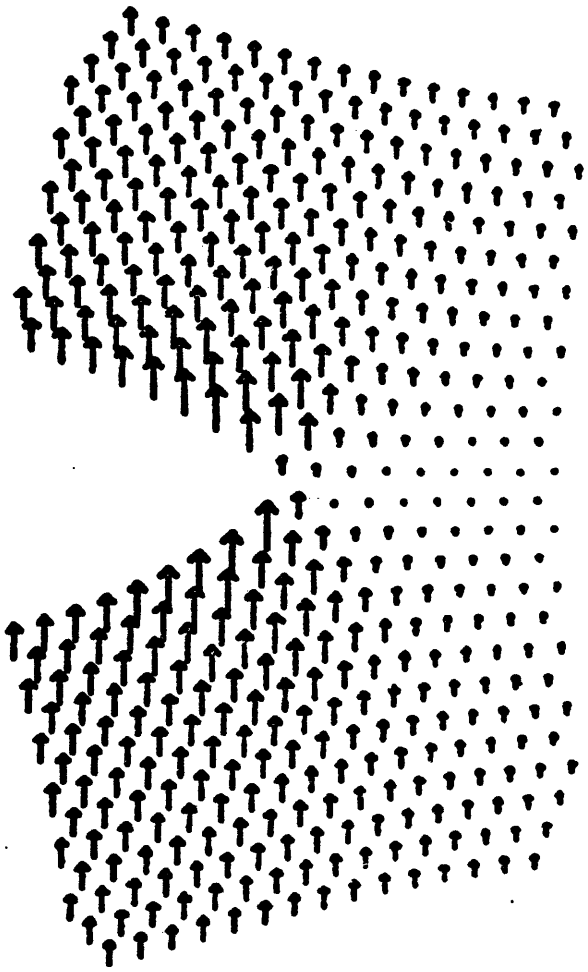

Figure 5.8a Rotations at the initial configuration (linear elasticity theory). ↑ indicates the magnitude of the rotation.

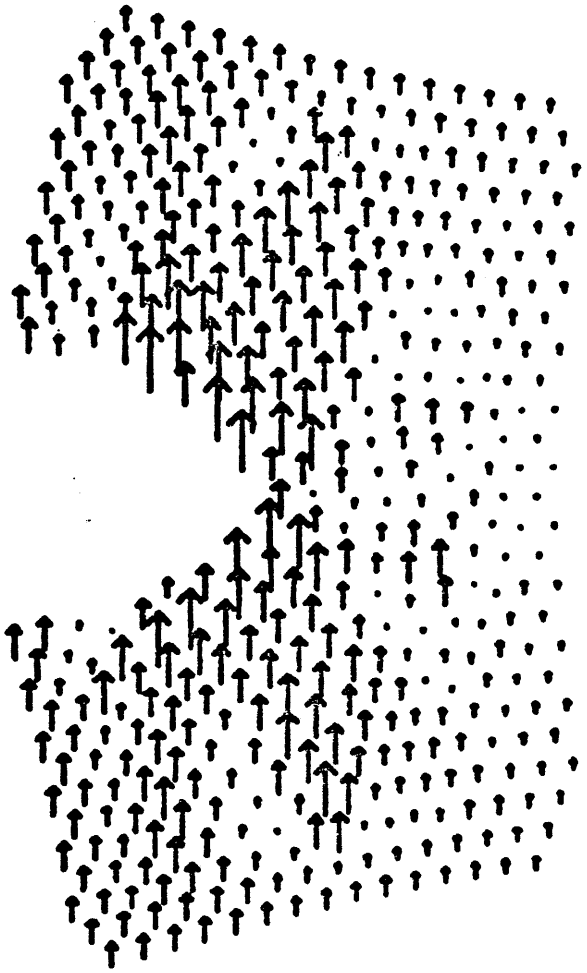

Figure 5.8b Rotations at the final relaxed configuration (fixed boundary). ↑ indicates the magnitude of the rotation.

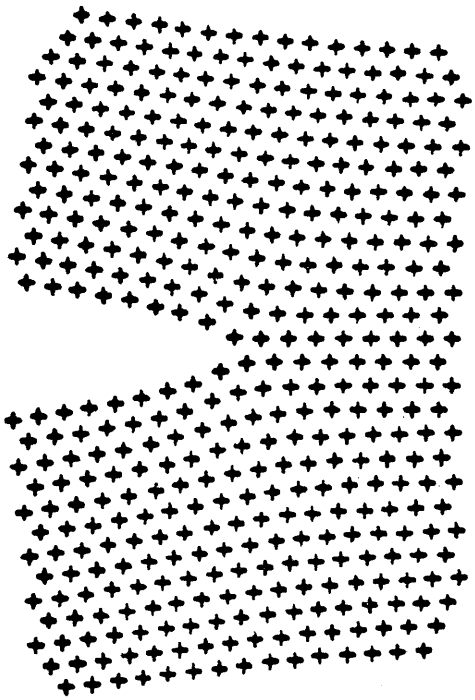

Figure 5.9a Initial atomic configuration (linear elasticity theory) Potential M-3. $K \simeq 0.5\, K_c$

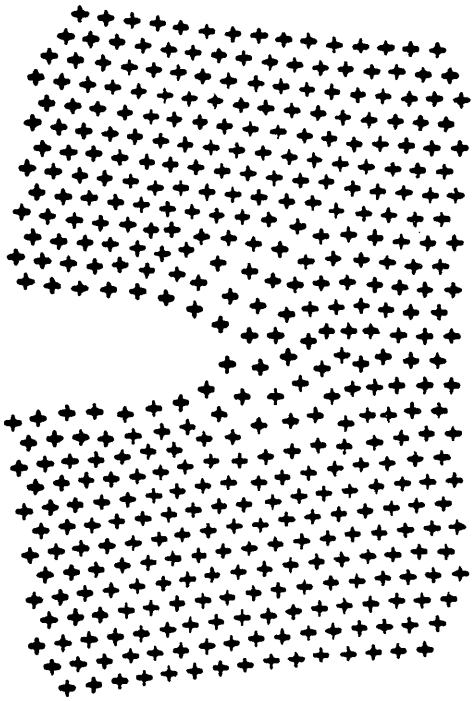

Figure 5.9b Final relaxed configuration (fixed boundary). Particles interact through a Morse potential (M-3). $K \simeq 0.5\ K_c$

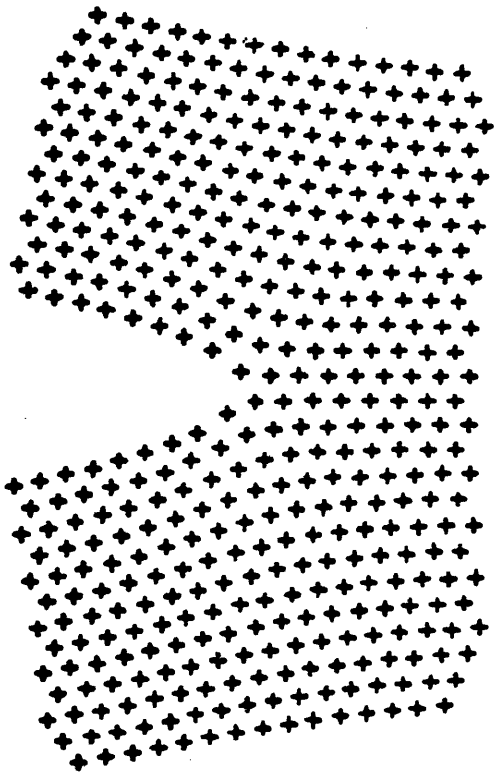

Figure 5.10a Initial configuration (linear elasticity theory). Potential M-2. $K \simeq K_c$

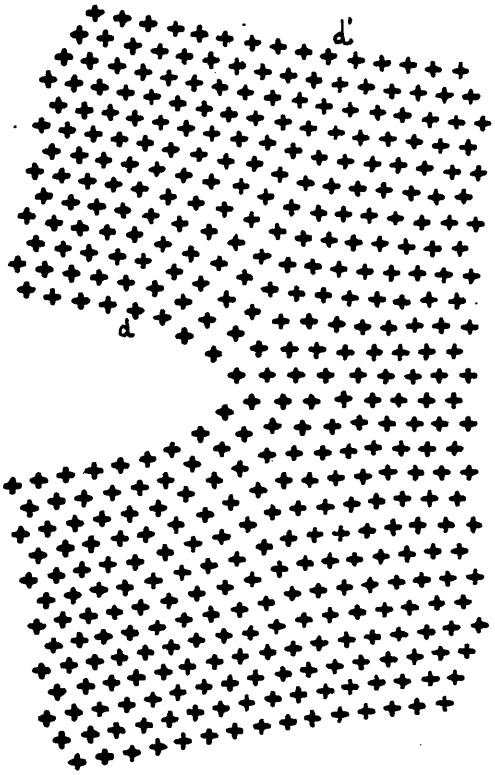

Figure 5.10b Final relaxed configuration (fixed boundary). Potential M-2.

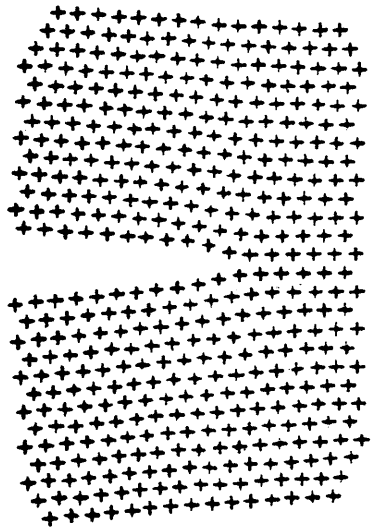

Figure 5.11 Atomic configuration during the application of flexible boundary. The critical stress has been exceeded and the crack propagates breaking bonds. Potential M-1.

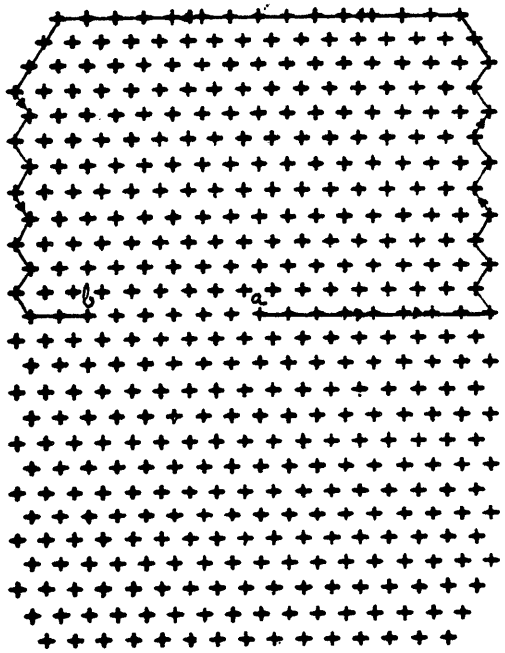

Figure 5.12 Burgers circuit in a perfect reference crystal. The circuit has been finished at point b to add all the Burgers vectors corresponding to shear on planes between points a and b. The same circuit has been applied to the final configuration (Fig. 5.6b) to determine the total Burgers vector.

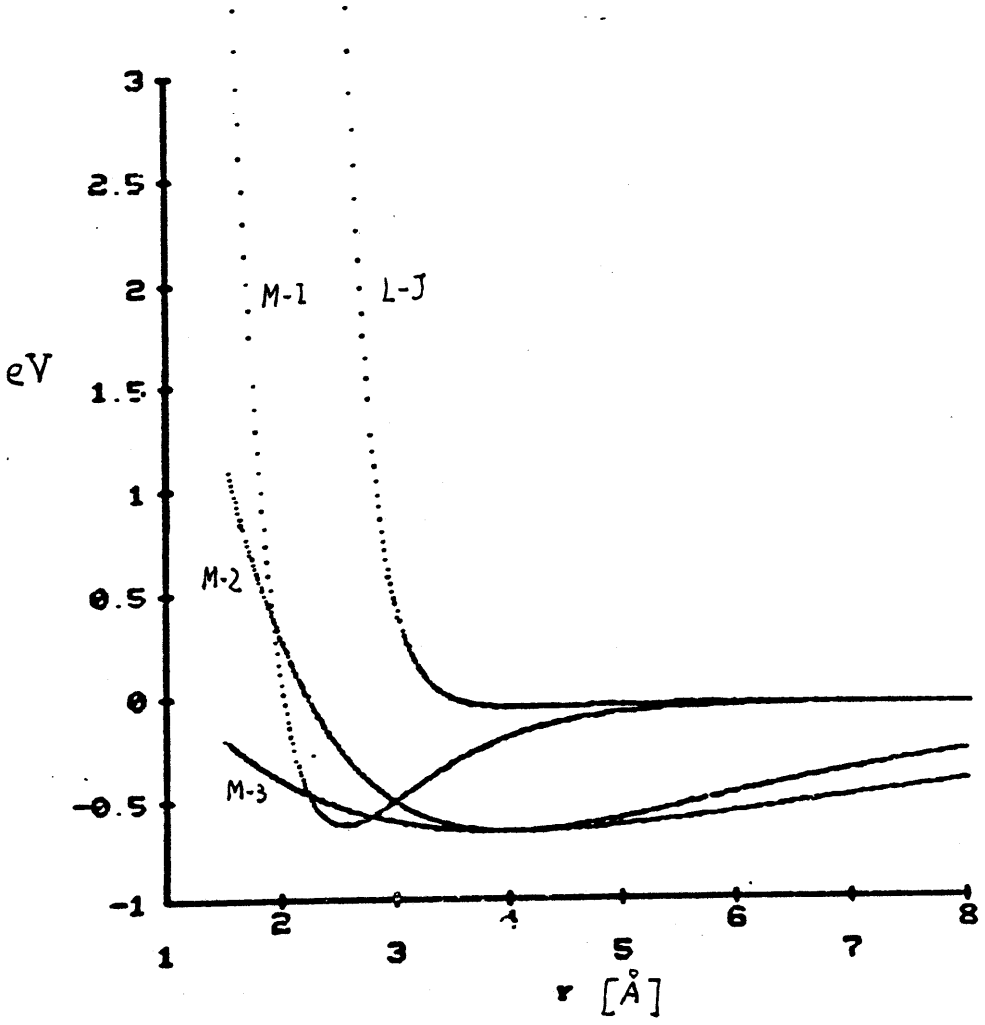

Figure 5.13 Potential functions used in the CMD simulations.

	Atomic spacing (Å)	Cut off range (Å)	μ shear modulus (2-D) dynes/cm	E Young's modulus (2-D) dynes/cm	γ surface energy (2-D) erg/cm	σ_{is} ideal shear stress (2-D) dynes/cm	σ_{ic} ideal cohesive stress 2-D dynes/cm	K_c critical stress intensity factor (2-D) dynes $cm^{-1/2}$
Morse $\alpha = 1.3543\ Å^{-1}$ M-1 $D = 0.5892$ eV $r_0 = 2.5475\ Å$	2.5475	3.7500	$1.50 \cdot 10^{4}$	$4.0 \cdot 10^{4}$	$2.393 \cdot 10^{-5}$	$1.62 \cdot 10^{3}$	$4.25 \cdot 10^{3}$	1.38
Morse $\alpha = 0.4\ Å^{-1}$ M-2 $D = 0.625$ eV $r_0 = 4.00\ Å$	3.2940	6.3000	$2.15 \cdot 10^{3}$	$5.73 \cdot 10^{3}$	$1.120 \cdot 10^{-5}$	$1.00 \cdot 10^{2}$	$1.52 \cdot 10^{3}$	$3.72 \cdot 10^{-1}$
Morse $\alpha = 0.25\ Å^{-1}$ M-3 $D = 0.625$ eV $r_0 = 4.00\ Å$	3.045	5.900	$1.10 \cdot 10^{3}$	$2.93 \cdot 10^{3}$	$3.480 \cdot 10^{-6}$	$0.60 \cdot 10^{2}$	$1.06 \cdot 10^{3}$	$1.42 \cdot 10^{-1}$
Lennard-Jones L-J $\epsilon = 165.9\ ^{\circ}K$ $\sigma = 3.679\ Å$	4.1295	6.2540	$4.18 \cdot 10^{2}$	$1.11 \cdot 10^{3}$	$4.660 \cdot 10^{-7}$	$0.51 \cdot 10^{2}$	$6.30 \cdot 10^{1}$	$3.22 \cdot 10^{-2}$

Table 5.1 Characteristic parameters and properties of several materials studied in CMD simulation.

		σ_{is}/σ_{ie}	KTC $\left[\frac{\sigma_{is}/\sigma_{ic}>0.5}{\text{brittle}}\right]$	ξ_o $\xi_o=\frac{1}{e^{3/2}(1-\nu)}=\frac{r_o}{b}$	ξ_c $\xi_c=\frac{r}{b}$	RT $[\xi_o<\xi_c$ brittle$]$	CMD
M-1	Morse $\alpha=1.3543\ \text{Å}^{-1}$ $D=0.5892$ eV $r_o=2.5475$ Å	0.38	Ductile	0.3346	1.75	Brittle	Brittle
M-2	Morse $\alpha=0.4$ $D=0.625$ eV $r_o=4.00$ Å	0.06	Ductile	0.3346	1.05	Brittle	Ductile
M-3	Morse $\alpha=0.25$ $D=0.625$ eV $r_o=4.00$ Å	0.05	Ductile	0.3346	1.40	Brittle	Ductile
L-J	Lennard-Jones $\varepsilon=165.9\ ^{\circ}$K $\sigma=3.679$ Å	0.81	Brittle	0.3346	3.75	Brittle	Brittle

Table 5.2 Predicted behavior according to Kelly, Tyson and Cottrell (KTC) criterion, Rice and Thomson (RT) criterion, and observed behavior by Computer Molecular Dynamics simulation (CMD).

Chapter Six

Summary and Conclusions

6. Summary and Conclusions

Computer Molecular Dynamics has been applied to the study of fracture in a two-dimensional lattice. The major purpose of this work was to study and establish interrelations between several macroscopic properties such as fracture toughness, stability of the crack against emission of dislocation and deformation field around the crack tip.

We have developed a computer simulation program which can be used with crystalline solids, liquids and gases, under a variety of boundary conditions, periodic, free, fixed and flexible boundaries.

The first step in the development of the computer simulation model consisted of setting up the standard CMD techniques which permitted an accurate and efficient determination of the classical trajectories of the particles and the static and dynamic properties of the system. The simulations were carried out in a perfect monoatomic system (rare gas). Additional tests were done to study the accuracy of the calculations: conservation of energy and reversibility of trajectories.

The microscopic elastic constants, dispersion relation and phonon spectrum of the system were determined by lattice dynamics. These calculations were not necessary for the rest of the work but of interest in order to study anharmonic effects and derive analytical expressions for calculating the macroscopic elastic constants of the system.

Two boundary conditions have been studied in detail. A fixed boundary condition consists of placing the boundary particles according to a continuum elasticity solution. A flexible boundary condition

consists of surrounding the simulation region by a continuum region in which particles are moved according to a Green's function to relax the forces arising from the interactions between the atomic system and the continuum. The Green's function used is that derived by Hirth for the case of isotropic elastic media with a crack, a result we have rederived for the case of a line force in an infinite medium following a procedure similar to the determination of potentials in electrostatics. The simplicity and generality of this method permit direct applications to the determination of the displacement fields of other point and line defects (i.e., interstitials and dislocations).

The flexible boundary procedure was found to be efficient and accurate in studying crack tip configurations in brittle materials. It was possible to determine the critical stress values for propagating the crack with a smaller number of particles compared to the fixed boundary method.

The critical stress intensity factor, determined by CMD simulation in brittle materials, has been found to be greater than the value predicted by Griffith's theory. However, this value is quite sensitive to the assumed crack surface interactions in the simulation. Higher values, about two times Griffith's predictions, were found when interactions were permitted between atoms situated on opposite crack surfaces, and lower values, about 15% greater than the Griffith criterion, were found when no interactions were assumed.

The difference between these results and Griffith's theory can be explained as follows. First, the Griffith criterion is based on an energy balance and it is considered a necessary but not sufficient

condition for crack propagation. Secondly, the equations used by Griffith are based upon macroscopic linear elastic continuum properties and do not consider the local atomic relaxations around the crack tip and the changes in stress distribution with different crack tip atomic models. In the case of plasticity we should include as another reason for the large critical stress found by simulation the additional energy expended in the emission of dislocations. In the test of Griffith's criterion we have worked with a brittle solid, a Lennard-Jones rare gas system. Other potentials appropriate for brittle materials or even truncated Hookean potentials would be interesting cases for study by CMD.

The flexible boundary method was found to be not so efficient, in the sense of being applicable to systems with small number of particles, when high stresses were applied and large non-linear regions were produced around the crack tip. The constraint imposed by the continuum solution at the boundaries does not permit one to study plastic relaxation by the emission of dislocation from the crack tip. However, this constraint was not so important during the first stages of the plastic region formation or when small stresses were applied. In these cases, the plastic region was small and did not interact with the boundaries.

The strain and rotation fields were determined for several stresses and different potential functions. The purpose of using different potential functions was to study the influence of the potential parameters on the brittle or ductile behavior observed by computer simulation.

In the case of ductile materials, which correspond to Morse potentials M-2 and M-3, emission of dislocation from the crack tip was observed and the size of the sheared region increased with higher applied stresses. In some of the results obtained with the potential M-3, analysis of the rotation field around the sheared region suggests a phase transition from triangular to cubic lattice.

The Kelly, Tyson and Cottrell (KTC) and Rice-Thomson (RT) criteria for predicting brittle or ductile behavior in crystalline materials were studied and their predictions confronted to CMD observation. Both criteria are based on continuum linear elastic derivations and in order to determine their predictions the elastic constants, surface energy and ideal stresses were calculated by independent simulations for all the potential functions.

The predictions of KTC criterion gave good agreement with CMD observations. In the case of the Morse potential M-1, which is more steeply repulsive compared to M-2 and M-3, the behavior is not well-defined. While the value of the ratio $\sigma_{is} / \sigma_{ic}$ is close to 0.5, the limit for ductile behavior, brittle behavior was observed in CMD results. However, the computer results also indicated strong interaction of shear deformation with the boundaries and this could have been the reason for the absence of dislocations in the data.

The RT criterion seems to underestimate the possibility of ductile behavior. However, more accurate predictions can be obtained by using CMD to determine more realistic values for the core of the dislocation. The core width, as it has already been discussed, can vary significantly with the slope of the potential function, the

width increasing with a steeper slope. This fact would explain again the absence of dislocations in the simulation with the M-1 potential, where the emission of dislocations would be prevented by the strong interaction of the wide and uncompressible core of the dislocation with the boundaries.

The brittleness of the material can be affected by the depth of the potential function, assuming no significant changes occur to other physical constants. The surface energy, or energy necessary to create a new surface by breaking bonds is logically connected with this parameter that determines the energy to break one atomic bond.

Further improvements in the study of emission and propagation of dislocations from the crack tip could be done by determining the Peirls stress and core width of the dislocation by CMD, using the potential functions studied in this thesis. The distance travelled by a dislocation in the presence of the crack tip stress field will depend ultimately on the stress necessary to overcome the friction of the lattice (Peierls stress), and it will define the extension of the plastic region. The width of the dislocation core would help to predict accurately the behavior of the system using the RT criterion and also would explain the influence of the boundaries on the emission of dislocations from the crack tip. Flexible boundary conditions could play an important role in the determination of the Peierls stress and core width of the dislocation. In this case our system would consist of a dislocation core, with a width of a few interatomic spacings, and an exterior linear elastic region that can be accurately treated with our flexible boundary procedure.

Another interesting area of future work is the dynamics of crack propagation. This problem is well suited to studies by CMD, but involves difficulties with regard to appropriate boundary conditions.

Finally, it is necessary to remark that all the present simulations were carried out with a two-dimensional system at 0°K. There are known physical properties such as the ductile behavior of Cu which may appear to be inconsistent with our simulation, in this case the results on Morse potential M-1. We do not think this is a real conflict because there are close packet planes in a three-dimensional system which are not present in a two-dimensional system. It would be desirable to verify directly by simulation that a three-dimensional solid with potential M-1 is indeed ductile. The consideration of this factor would not involve great computational difficulties and could be another area of future work.

References

Chapter One

1. E. Orowan, Rep. Progr. Phys. 12, 48(1949).

2. P.C. Gehlen and M.F. Kanninen, "Inelastic Behavior of Solids", edited by M.F. Kanninen, McGraw-Hill, New York (1970).

3. J.E. Sinclair and B.R. Lawn, Proc. Roy. Soc. London A329, 83(1972).

4. W.T. Sanders, Eng. Fract. Mech. 4, 145(1972).

5. J.H. Weiner and M. Pear, J. Appl. Phys. 46, 2398(1975).

6. W.T. Ashurst and W.G. Hoover, Phys. Rev. B14, 1065(1976).

Chapter Two

1. J.E. Lennard-Jones, Proc. R. Soc. A106, 463(1924).

2. P.M. Morse, Phys. Rev. 34, 57(1929).

3. L.A. Girifalco and W.G. Weizer, Phys. Rev. 114, 687(1958).

4. P. Shofield, Computer Physics Communications 5, 17(1973).

5. P.C. Gehlen, J.R. Beeler and R.I. Jaffee, "Interatomic Potentials and Simulation of Lattice Defects", (1972).

6. J.R. Beeler, Jr., in "Advances in Materials Research", Vol. 4, H. Herman/John Wiley & Sons (1970), pp. 295-476.

7. P.A. Flinn and A.A. Maradudin, Ann. Phys. (NY) 18, 81(1962).

8. H. Kanzaki,J. Phys. Chem. Solids 2, 24(1957).

9. J.R. Hardy, J. Phys. Chem. Solids 15, 39(1960).

10. J.B. Gibson and A.N. Goland, Phy. Rev. 120, 1229(1960).

Chapter Three

1. A.A. Griffith, Phil. Trans. Roy. Soc. A221, 163(1920).

2. A.A. Griffith, Proc. First Internat. Congr. Appl. Mech. (ed. C.B. Biezeno), p. 55.

3. C.E. Inglis, Trans. Inst. Naval Archt. 55, 219(1913).

4. A.J.M. Spencer, Int. J. Engng. Sci. 3, 441(1965).

5. A. Kelly, W. Tyson and A.H. Cottrell, Phil. Meg. 15, 567(1967).

6. J.R. Rice and R. Thomson, Phil. Mag. 29, 78(1974).

7. M.F. Kanninen and P.C. Gehlen, "Interatomic Potentials and Simulation of Lattice Defects", J.R. Beeler (Plenum, N.Y. 1972), p. 7B.

8. P.C. Gehlen and M.F. Kanninen, "Inelastic Behavior of Solids", P.C. Gehlen, editor (1970).

9. M.F. Kanninen and P.C. Gehlen, Int. Journ. of Fracture Mech. 7, 471(1971).

10. J.E. Sinclair and B.R. Lawn, Proc. R. Soc. Lond. A329, 83*1972).

11. R. Thomson, C. Hsieh and V. Rana, J. Appl. Phys. 42, 3154(1971).

12. R. Thomson, Ann. Rev. Mat. Sci. 3, 31(1973).

13. C. Hsieh and R. Thomson, J. Appl. Phys. 44, 2051(1973).

14. A. Gohar, "A Microscopic Fracture Study in the 2-D Triangular Lattice", thesis (1979).

15. W.T. Ashurst and W.G. Hoover, Phys. Rev. B14, 1465(1976).

16. J.H. Weiner and M. Pear, Journal of Appl. Phys. 46, 2398(1975).

Chapter Four

1. J.E. Sinclair, P.C. Gehlen, R.G. Hoagland and J.P. Hirth, J. Appl. Phys. 49, 3890(1978).

2. J.E. Sinclair, Philos. Mag. 31, 647(1975).

3. P.C. Gehlen, J.P. Hirth, R.G. Hoagland and M.F. Kanninen, J. Appl. Phys. 43, 3921(1972).

4. P.C. Gehlen, G.T. Hahn and M.F. Kanninen, Scripta Met. 6, 535(1972).

5. A.J. Markworth, M.F. Kanninen and P.C. Gehlen, Int. Conf. of Stress Corrosion Cracking, France (12 June 1973).

6. R.G. Hoagland, J.P. Hirth and P.C. Gehlen, Philos. Mag. 34, 413(1976).

7. J.P. Hirth and J. Lothe, "Theory of Dislocations", McGraw-Hill (1968).

8. J.P. Hirth, R.G. Hoagland and P.C. Gehlen, Int. J. Solids Structures 10, 977(1974).

9. J.P. Hirth, Scripta Met. 6, 535(1972).

10. A.E. Green and W. Zerna, "Theoretical Elasticity", Oxford Press (1954).

11. G.C. Sih and A. Liebowith, "Fracture", (1968).

12. N.I. Muskhelishvili, "Some Basic Problems in the Mathematical Theory of Elasticity", Nordhoff, Groningen, Holland (1953).

13. N.I. Muskhelishvili, "Singular Integral Equations", Nordhoff, Groningen, Holland (1953).

14. B.R. Lawn and T.R. Wilshaw, "Fracture of Brittle Solids", Cambridge University Press (1975).

15. J.D. Eshelby, W.T. Read and W. Shockley, Acta Met. 1, 251(1953).

16. W.T. Ashurst and W.G. Hoover, Phys. Rev. B14, 1465(1976).

17. W.G. Hoover, W.T. Ashurst and R.J. Olness, J. Chem. Phys. 60, 4043(1974).

18. L.D. Landau and E.M. Lifshitz, "Theory of Elasticity", Pergamon, New York (1959).

19. A. Love, "The Mathematical Theory of Elasticity", Cambridge University Press, Cambridge (1927).

20. A.S. Argon and H.Y. Kuo, Mat. Sci. Engng. 39, 101(1979).

21. A.H. Cottrell, "Dislocations and Plastic Flow in Crystals", (1953).

22. P.C. Gehlen, G.F. Hahn and M.F. Kanninen, Scripta Met. 6, 1087(1972).

Chapter Five

1. J.R. Rice and R. Thomson, Phil. Mag. 29, 73(1974).

2. A. Kelly, W.R. Tyson and A.H. Cottrell, Phil. Mag. 15, (1967).

3. J. Hirth and J. Lothe, "Theory of Dislocations" (McGraw-Hill) 1968, p. 212.

4. J. Cottrell, "Lattice Defects and Their Interactions", R.R. Hanguti, Gordon and Breach, Science Publishers, New York (1968).

5. L.A. Girifalco and V.G. Weizer, Phys. Rev. 114, 687(1959).

6. J. Frenkel, Zeit. Phys. 37, 572(1926).

7. A.H. Cottrell, "Dislocations and Plastic Flow in Crystals" (1953), p. 10.

8. A.S. Argon and H.Y. Kuo, Mat. Sci Engng. 39, 101(1979).